PERIODICO di MINERALOGIA
established in 1930

DIPARTIMENTO
DI SCIENZE DELLA TERRA

SAPIENZA
UNIVERSITÀ DI ROMA

An International Journal of
Mineralogy, Crystallography, Geochemistry,
Ore Deposits, Petrology, Volcanology
and applied topics on Environment, Archaeometry and Cultural Heritage

Petrological characterization of the Cenozoic igneous rocks of the Tafresh area, central Urumieh-Dokhtar Magmatic Arc (Iran)

Giulia Salari [1], Michele Lustrino [1,2], Mohammad Reza Ghorbani [3], Samuele Agostini [4], Lorenzo Fedele [5,*]

[1] Department of Earth Sciences, Sapienza University of Rome - P.le A. Moro 5, 00185, Rome, Italy
[2] CNR - Institute of Environmental Geology and Geoengineering (IGAG), c/o Department of Earth Sciences, Sapienza University of Rome - P.le A. Moro 5, 00185, Rome, Italy
[3] Department of Geology, Tarbiat Modares University, Tehran 14115-175, Iran
[4] CNR - Institute of Geosciences and Georesources (IGG), Via Giuseppe Moruzzi 1, 56124, Pisa, Italy
[5] Department of Earth, Environmental and Resources Sciences (DiSTAR), University of Naples Federico II - Via Cintia 21, 80126 Naples, Italy

ARTICLE INFO

Submitted: April 2020
Accepted: July 2020
Available on line: October 2020

* Corresponding author:
lofedele@unina.it

DOI: 10.13133/2239-1002/16620

How to cite this article:
Salari G. et al. (2021)
Period. Mineral. 90, 59-83

ABSTRACT

We report a petrographic and whole-rock geochemical characterization of the Cenozoic igneous rocks cropping out in the Tafresh area, central Urumieh-Dokhtar Magmatic Arc, NW Iran. The investigated rocks range mainly from basaltic andesite to dacite, and are considered to be genetically linked to a three-step, (mostly) closed-system evolutionary process. It involves first the fractionation of ferromagnesian minerals (mainly clinopyroxene and olivine) and plagioclase, followed by a second removal of plagioclase and lesser amphibole (plus minor clinopyroxene) and eventually, in the most evolved phases, the crystallization of plagioclase with lesser alkali feldspar and minor amphibole. Tafresh rocks define a typical calcalkaline series generated from a subduction-modified mantle wedge, characterized by the classical LILE-enriched and HFSE-depleted compositions. The basaltic andesite magmas do not represent primitive compositions, but are likely derived from an unsampled hydrous primitive melt equilibrated in a spinel-bearing metasomatized peridotite source, evolving at shallow to moderate crustal depths. Additional lithotypes cropping out in the Tafresh area include much rarer strongly evolved leucocratic rocks and evolved rocks with adakitic signature. The first are thought to derive from crustal anatexis of a meta-sedimentary source, whereas the latter are interpreted as the product of the melting of a meta-mafic source rock with residual garnet and amphibole. The association of magmatic rocks pointing to all such different petrogenetic processes in a relatively limited area is strongly suggestive of emplacement in a post-collisional stage.

Keywords: Urumieh-Dokhtar; Zagros; subduction-related magmatism; calcalkaline series; adakites.

INTRODUCTION

The Urumieh-Dokhtar Magmatic Arc is a NW-SE trending sector in W Iran where an extensive Cenozoic igneous activity developed as a consequence of the NE-directed subduction of the Neotethyan Ocean. This oceanic lithosphere was originally located in between the Arabian and Eurasian plates, and its closure eventually culminated in the built-up of the Bitlis-Zagros Orogen in Eastern Anatolia and Western Iran, respectively (e.g., Agard et al., 2011 and references therein). As part of

the Alpine-Himalayan Belt, the Zagros Orogen has experienced a complex geodynamic evolution, which stimulated a number of geological investigations on several interconnected topics dealing with geophysics, active tectonics, igneous and metamorphic response, as well as sedimentary evolution (e.g., Agard et al., 2005; Molinaro et al., 2005; Mouthereau et al., 2006, 2012; McQuarrie and van Hinsbergen, 2013; Koshnaw et al., 2018; Karasözen et al., 2019; Rabiee et al., 2020).

Nevertheless, compared with its western (i.e., Alps) and eastern (Himalayas) counterparts, the Zagros Orogen remains less documented, and numerous are the topics that still need to be resolved (e.g., the timing of collision, the position of the suture zone, and the chronological, chemical and spatial evolution of the igneous activity). In such a framework, multidisciplinary geological studies are extremely useful to unravel the uncertainties that still characterize the geodynamic reconstructions of the area, similarly to what has been proposed in the western Alpine-Himalayan Belt (e.g., Carminati et al., 2012; Faccenna et al., 2014; van Hinsbergen et al., 2020).

A major source of information is represented by the petrological features inferred from petrography and whole-rock geochemistry of the igneous rocks emplaced during the geological evolution of the orogenic belt. In the Zagros Orogen case, information regarding the associated long-lasting magmatism, occurred in the two subparallel NW-SE-oriented magmatic belts of the Sanandaj-Sirjan Magmatic Arc (SSMA) and the Urumieh-Dokhtar Magmatic Arc (UDMA), covering more than 150 Myr (e.g., Omrani et al., 2008; Chiu et al., 2013), remains, however, relatively limited.

The purpose of this work is to present a petrological characterization of the igneous rocks cropping out in the Tafresh area, in the central portion of the Urumieh-Dokhtar Magmatic Arc. This will contribute to increase the petrological knowledges about the magmatism associated with the built-up of the Zagros Orogen and possibly provide additional constrains to the models proposed for the geodynamic evolution of the area.

GEOLOGICAL BACKGROUND

The basement of the Iranian plate is made of numerous continental terranes (the *Cimmerian continent collage*; Sengör et al., 1988) that peeled off the NE margin of Gondwana since the Early Permian (e.g., Stampfli et al., 2013). The NE-directed drift of the Cimmeria terrane ended in the Norian, when the old Paleotethys Ocean, originally to the NE of Cimmeria, was completely subducted NE-ward beneath the southern Eurasian paleo-margin, marking the Cimmeria-Eurasia continental collision stage along the Albortz Mountains belt (Hassanzadeh et al., 2008; Wilmsen et al., 2009; Verdel et al., 2011; Stampfli et al., 2013). Concomitantly with the NE-directed continental drift of Cimmeria, a new oceanic basin (Neotethys Ocean) started to develop. The early Cretaceous-Miocene subduction of this ocean, as well as that of the westernmost Jurassic oceanic basin of Alpine Tethys, define the central-western sectors of the Alpine-Himalaya orogenetic belt, whose easternmost continuation is associated to the Late Paleocene India-Eurasia collision (van Hinsbergen et al., 2019).

The Norian closure of the Paleotethys Ocean is now identifiable in a discontinuous suture zone cropping out along northern Iran, from northern Alborz Mountains, South of Caspian Sea, to northern Binalud Mts., close to the boundary with Afghanistan and Turkmenistan; Figure 1). The Neotethys Ocean started to subduct NE-ward beneath the Iranian plate, thus leading to the partial melting of the mantle wedge and to the genesis of the magmas responsible for the built up of the SSMA (e.g., Berberian and Berberian, 1981; Berberian and King, 1981; Arvin et al., 2007; Wilmsen et al. 2009; Agard et al., 2011; Chiu et al., 2013; Burg, 2018). Magmatism in the SSMA is mostly of Mesozoic age but comprises also scattered Paleocene to Upper Eocene manifestations (~60-35 Ma; Mazhari et al., 2009; Azizi et al., 2011; Mahmoudi et al., 2011; Chiu et al., 2013). The emplaced products include both volcanic and plutonic rocks, mostly with calcalkaline affinity, classically interpreted to reflect an Andean-type arc system (e.g., Berberian and Berberian, 1981; Agard et al., 2005, 2011; Shahbazi et al., 2010; Hassanzadeh and Wernicke, 2016; Deevsalar et al., 2017).The continuing north-eastward subduction of the Neotethys Ocean beneath the SW margin of the Iranian continent finally led to the collision between Arabia and Iran, marking the beginning of the Bitlis-Zagros fold-and-thrust belt build-up (Figure 1; e.g., Agard et al., 2011). The exact timing of such collisional event is debated, as several different lines of evidence provide estimates spanning a ~175 Myr time interval [i.e., from Upper Triassic to Miocene; e.g., Agard et al. (2011), Verdel et al. (2011), Koshnaw et al. (2018)]. Detailed zircon U-Pb age data on the igneous products associated with this phase argue for an oblique convergence, which thus resulted in a progressively younger onset of the continental collision moving from NW towards SE Iran (i.e., from ~22 to ~10-6 Ma; Chiu et al., 2013). This is also in line with present-day kinematic data (indicating Arabia-Eurasia convergence ~20-30° oblique to the Zagros orogen; Masson et al., 2007) and with the still active oceanic subduction in the Makran zone, at the south-easternmost tip of Iran (e.g., Burg, 2018).

As previously mentioned, during such a geodynamic evolution, a diffuse calcalkaline magmatism developed along the western margin of Iran during the Cenozoic,

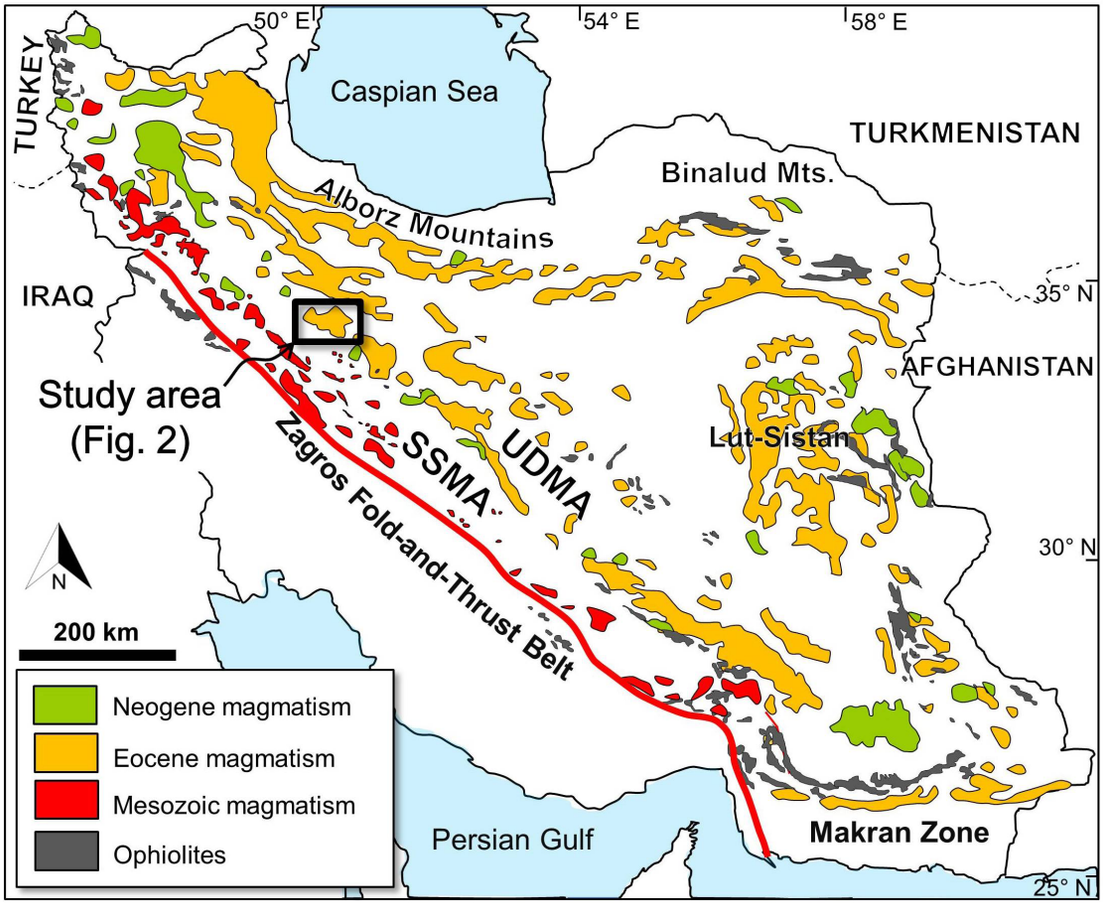

Figure 1. Simplified geological sketch map of Iran (after Shafaii Moghadam et al., 2016) with bold black rectangle indicating the location of the Tafresh study area (for which a highlight is provided in Figure 2).

mostly along the UDMA. Other igneous districts related to the Arabia collision crop out in eastern Anatolia (e.g., Di Giuseppe et al., 2017; Karaoğlu et al., 2020), the Lesser Caucasus/Alborz belt (northern Iran, where it merges with north-western UDMA; e.g., Asiabanha and Foden, 2012), Central Iran and the Lut-Sistan region (easternmost Iran; e.g., Pang et al., 2013; Figure 1).

The UDMA runs for ~1500 km in western Iran with a NW-SE orientation approximately parallel to the Zagros main thrust and the SSMA. Magmatism peaked during the Eocene, emplacing products with calcalkaline (plus rarer transitional shoshonitic) affinity and the typical geochemical signature of subduction-related magmas (e.g., Omrani et al., 2008; Verdel et al., 2011). A more detailed geochronological scheme for UDMA magmatism is that proposed by Chiu et al. (2013) based on an extensive zircon U-Pb geochronology study. According to these authors, the earliest (81-72 Ma) magmatic manifestations occurred in SE UDMA, followed by a prolonged quiescent period. Magmatism reprised with widespread Eocene activity, reaching its peak of intensity in the 55-25 Ma time span (Lower Eocene-Upper Oligocene) and then progressively ceasing from NW to SE. In addition, subsequent to the ~Oligocene continental collision, less diffuse episodes of magmatic activity across the Arabia-Eurasia suture zone mostly concentrated towards the Anatolian border during Pliocene-Quaternary times (e.g., Davidson et al., 2004; Walker et al., 2009; Allen et al., 2013). Such magmatic activity was quite variable in terms of magma composition (from basic to evolved, including adakitic types), serial affinity (from calcalkaline to alkaline, plus lesser shoshonitic and ultrapotassic) and even geochemical signature, varying from subduction-related to within-plate-like (e.g., Pearce et al., 1990; Davidson et al., 2004; Jahangiri, 2007; Omrani et al., 2008; Kheirkhah et al., 2009, 2013; Walker et al., 2009; Ahmadzadeh et al., 2010; Lustrino et al., 2010, 2019; Verdel et al., 2011; Allen et al., 2013; Neill et al., 2015; Fazlnia, 2019). The switch in geochemical signature has been alternatively attributed to the onset of asthenospheric

upwelling (resulting from slab roll-back and thinning of the lithosphere; Verdel et al 2011), or to a change in the mineralogy of the metasomatized lithospheric mantle (related with the disappearance of amphibole from the refractory residue; Allen et al. 2013).

SAMPLING AREA AND ANALYTICAL TECHNIQUES

The investigated rocks were collected in the Tafresh area, at the northwestern tip of the central UDMA (Figure 1). According to the 1:100,000 Geological Maps of Tafresh (Hajian, 1977) and Farmahin (Hajian, 1970), the igneous rocks are mainly massive lavas and pyroclastic deposits with amphibole-rich andesitic composition, intruded by dykes and dioritic/granitoid bodies and associated sedimentary strata. A stratigraphic type-sequence for the central/north-western UDMA is exposed in the Tafresh area (Verdel et al., 2011), beginning with Mesozoic carbonatic and silicilastic deposit, covered by Paleocene-Eocene volcanic and sedimentary deposits, and by the Upper Eocene to Lower Oligocene sedimentary and subordinate volcanic deposits of the Lower Red Formation. The sequence continues with the Oligocene to Lower Miocene Qom Formation, made of shallow marine carbonates and mafic volcanic rocks, then by Miocene gypsum deposits of the Upper Red Formation, and is closed by Pliocene-Quaternary continental deposits.

Regionally, the study area was affected by reverse and dextral faulting associated with thrusting of the Eocene volcano-sedimentary series over the Qom Formation and Pliocene conglomerates (Hajian, 1977; Raeisi et al., 2019). The dominant NW-SE striking of the thrusts is parallel to the regional tectonic fabric of the UDMA, with minimum perpendicular stresses allowing the emplacement of near E-W trending granitoid magmas (Raeisi et al., 2019).

The earliest geochronological estimates for the Tafresh area igneous rocks were mainly based on the fossiliferous record of the interbedded sedimentary deposits, suggesting an Eocene age (Hajian, 2001). Whole-rock K-Ar absolute age data for two adakitic rocks and one basaltic lava sample range from Upper Oligocene (~27 Ma) to Middle Miocene (~15 Ma; Ghorbani et al., 2014). A Lower Miocene zircon U-Pb age of 17.4 Ma has been provided for a granodioritic body from the nearby Qom locality (Chiu et al., 2013). Significantly older U-Pb and $^{40}Ar/^{39}Ar$ ages have been also reported by Verdel et al. (2011), covering approximately the 57 to 44 Ma time interval (i.e., Upper Paleocene to Middle Eocene).

Twenty-five rock samples were collected close to the city of Tafresh (eastern part of the Markazi Province, ~160 km SW of Tehran). One additional sample (F1-46) was collected ~20 km NE of Tafresh and ~30 km SW of Saveh, ~15 km from the main sampling location (Figure 2). Samples were prepared for petrographic and geochemical characterization at the laboratories of the Dipartimento di Scienze della Terra of Sapienza Università di Roma. Rocks were cut using a diamond disc saw and then ground in a steel jaw crusher. Rock chips were washed with distilled water, dried overnight in an oven at ~60 °C, hand-picked under binocular stereomicroscope to remove the most altered portions, and eventually pulverized in a low-blank agate mortar. Whole-rock major and trace element contents and weight loss on ignition (LOI) were determined respectively by mixed ICP-AES (Inductively Coupled Plasma-Atomic Emission Spectrometry) and ICP-MS (Inductively Coupled Plasma-Mass Spectrometry) and by standard thermogravimetric techniques, at Actlabs (Ontario, Canada). Results are reported in Tables 1 and 2. Average detection limits range from 0.001 to 0.01 % from major elements, 0.1 to 30 ppm for trace elements and from 0.004 to 0.1 ppm for REE. Full analytical details can be found at www.actlabs.com.

RESULTS

Petrography

Tafresh igneous rocks are generally not well preserved, with abundant secondary phases partially to totally replacing primary minerals, and some calcite veins in the deeply altered samples (related to interaction with hydrothermal fluids and/or superficial weathering). A rough first-level distinction can be made between four groups of rock samples with different degrees of evolution, as inferred from mineral paragenesis and phase abundances (Figure 3).

Weakly evolved rocks (samples F1-22, F1-33, F1-36, F2-12, F2-34, F3-24, F4-49, F4-58) generally show a fine/moderate-grained holocrystalline intergranular doleritic texture, almost entirely made by plagioclase and ferromagnesian minerals (plus accessory opaques) in approximately similar proportions (Figure 3a). Plagioclase laths are generally better preserved (in some samples occurring also as few larger phenocrysts) with respect to mafic phases, with the latter being generally not easily distinguishable as they are totally replaced mainly by serpentine minerals or serpentine and calcite, more rarely by chlorite. Relatively fresh (or only partially replaced) crystals of clinopyroxene, fewer olivine and rare amphibole can be occasionally observed. Large plagioclase crystals (up to 1.2 cm in length and sometimes with "clast-like" appearance, possibly xenocrystic in origin) have been also recognized in samples F3-24 and F4-58. *Intermediate rocks* (F1-9, F1-11A, F1-11B, F1-13, F3-6, F3-13, F3-23, F4-1, F4-10, F4-11, F4-15) display both moderately to strongly porphyritic (with both microcrystalline and devitrified groundmass; Figure 3 b,c) and holocrystalline fine- to moderate-grained hypidiomorphic textures (plus fewer finer-grained

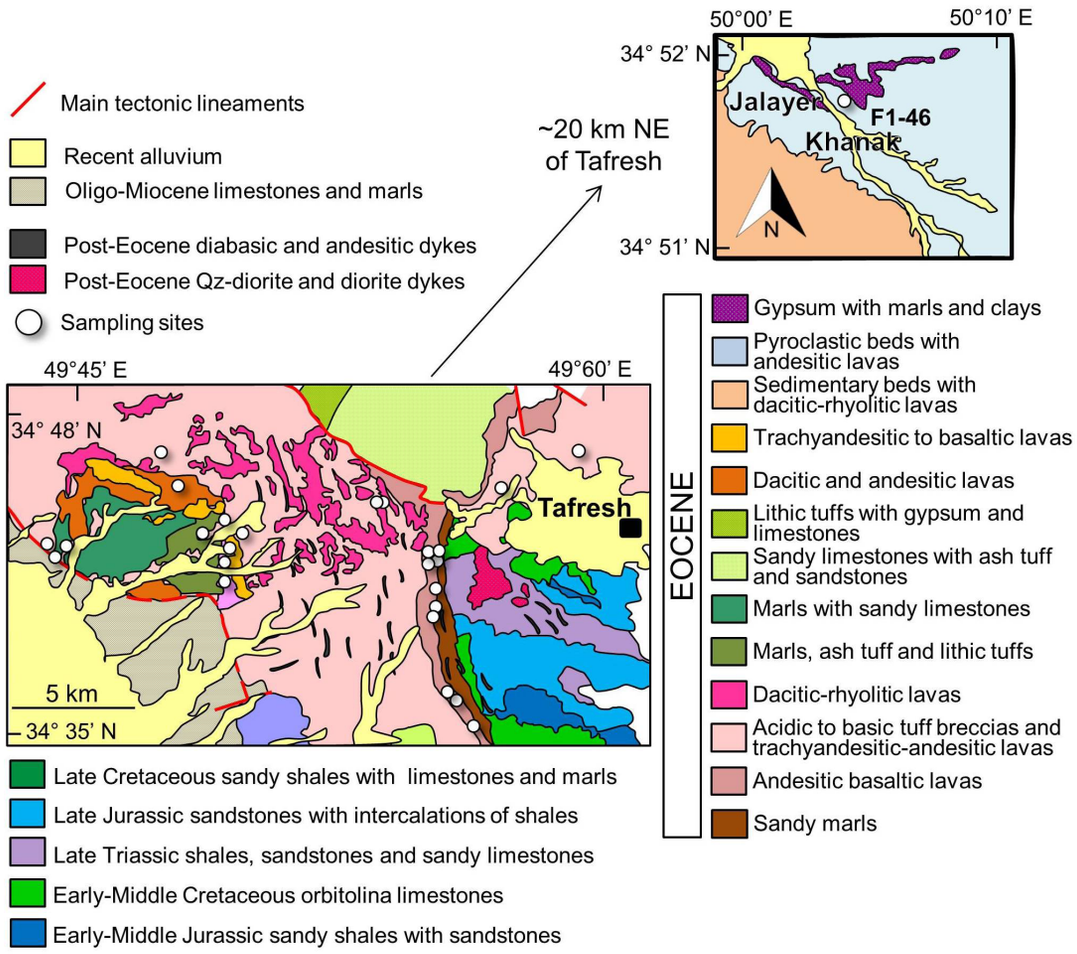

Figure 2. Simplified geological sketch map of the Tafresh area (after Hajan, 1970, 1977) with white dots indicating sample sites.

intergranular; Figure 3d) dominated by plagioclase and amphibole. Plagioclase is the most abundant phase, occasionally present also as larger phenocrysts or grains up to 6 mm in length (Figure 3b) and in monomineralic glomerules. Amphibole is the main mafic mineral (Figure 3 b,c,d), occurring both as fresh crystals and partially replaced by chlorite and calcite aggregates, sometimes forming larger phenocrysts/grains up to 5 mm in length. In samples F1-11A and F4-1, large anhedral amphibole (~3-4 mm in length, likely xenocrystic), in some instances poikilitically enclosing plagioclase laths (up to 8 mm in diameter, likely representing cumulitic intergrowths), are also observed. Rarer clinopyroxene crystals, mostly replaced by serpentine and calcite aggregates, and accessory opaques are also present.

Evolved rocks (F1-8, F1-29, F1-46) show moderately porphyritic (with devitrified groundmass) to holocrystalline fine/moderate-grained intergranular textures dominated by feldspar crystals plus fewer ferromagnesian minerals (Figure 3e). Plagioclase is still the main phase, forming large crystals up to 6 mm in length. Some alkali feldspar is also present, sometimes as large phenocrysts (~4 mm in length) or making monzonitic glomerules with plagioclase. The main mafic mineral is amphibole, commonly found as phenocrysts/grains (~3-4 mm) partially or totally replaced by chlorite or aggregates of chlorite and calcite/clay minerals. A few large biotite phenocrysts (~2 mm in length) have been found in sample F1-46. Opaque minerals are diffusely present as an accessory phase, occasionally as larger microphenocrysts/grains (up to 1 mm in diameter).

Strongly evolved rocks (F1-17, F1-18, F2-21, F3-3) have weakly- to moderately-porphyritic textures, generally with devitrified groundmass, and a remarkably leucocratic paragenesis dominated by plagioclase, alkali feldspar and quartz (Figure 3f). Ferromagnesian minerals are extremely rare, typically represented by sparse amphibole microcrysts, commonly altered to chlorite and/

Table 1. Major element concentrations (in wt% of oxide), LOI (in wt%) and CIPW-normative mineralogy (in vol%, calculated assuming $Fe_2O_3/FeO=0.15$) for the investigated rock samples from the Tafresh area with different degree of evolution and preservation (see text). Normative minerals: qtz=quartz; cor=corundum; or=orthoclase; ab=albite; an = anorthite; ne = nepheline; di = diopside; hy=hypersthene; ol=olivine; mt=magnetite; il=ilmenite; ap=apatite.

sample	F2-12	F2-34	F1-22	F3-24	F4-49	F4-58	F1-33	F1-36	F1-11A	F1-11B	F3-6	F3-13	F4-1	F4-10
geographic coordinates	34°38'N 49°54' E	34°42'N 49°56'E	34°41'N 49°43' E	34°41'N 49° 43' E	34°45'N 49°43' E	34°42'N 49°45' E	34°41'N 49°47' E	34°43'N 49°59' E	34°39'N 49°55' E	34°39'N 49°55' E	34°39'N 49°54' E	34°43'N 49°47' E	34°39'N 49°55' E	34°39'N 49°54' E
lithotype	weakly evolved								intermediate					
preservation	fresh		spoiled				altered		fresh					
SiO_2	53.81	53.89	50.89	51.67	50.46	50.68	48.98	44.69	56.31	56.86	59.23	58.23	55.28	57.53
TiO_2	0.90	0.90	1.09	0.92	0.89	0.83	1.45	1.12	0.75	0.74	0.62	0.89	0.81	0.68
Al_2O_3	17.59	17.64	18.90	18.76	16.66	19.21	13.66	16.61	18.19	17.41	17.88	16.27	18.12	16.96
Fe_2O_{3tot}	8.63	8.74	6.87	6.39	9.80	5.45	13.48	9.71	7.57	7.24	7.00	8.17	7.95	6.86
MnO	0.17	0.17	0.11	0.12	0.11	0.14	0.17	0.14	0.17	0.14	0.11	0.15	0.16	0.18
MgO	4.10	4.12	2.23	1.44	2.78	1.16	3.62	2.32	2.94	2.81	2.85	2.74	3.65	2.52
CaO	5.84	5.85	10.60	12.11	8.96	12.76	5.45	13.86	7.00	5.89	5.57	5.76	7.57	5.22
Na_2O	4.01	4.00	3.08	2.93	2.29	2.96	3.70	2.27	3.40	3.70	3.39	3.12	3.09	3.94
K_2O	1.48	1.48	0.47	0.64	0.72	0.91	0.47	0.50	0.97	2.18	0.91	1.47	0.87	1.31
P_2O_5	0.24	0.24	0.18	0.15	0.11	0.14	0.27	0.09	0.16	0.14	0.14	0.14	0.18	0.21
LOI	3.68	3.62	5.61	5.34	6.12	4.84	9.09	9.48	2.85	2.98	3.28	3.95	2.76	3.57
Total	100.50	100.60	100.00	100.50	98.90	99.07	100.30	100.80	100.30	100.10	101.00	100.90	100.50	98.98
qz	2.54	2.53	5.70	6.41	8.81	4.30	3.57	0.00	10.36	7.60	16.67	14.72	9.33	11.92
cor	0.00	0.00	0.00	0.00	0.00	0.00	0.00	0.00	0.00	0.00	1.56	0.00	0.00	0.08
or	9.04	9.01	2.94	3.98	4.59	5.71	3.04	3.24	5.88	13.27	5.50	8.96	5.26	8.11
ab	35.06	34.88	27.60	26.06	20.88	26.58	34.31	19.81	29.52	32.24	29.36	27.23	26.77	34.94
an	26.48	26.60	38.51	38.00	35.62	38.67	21.13	36.86	32.33	25.19	27.35	26.87	33.79	25.70
ne	0.00	0.00	0.00	0.00	0.00	0.00	0.00	0.67	0.00	0.00	0.00	0.00	0.00	0.00
lc	0.00	0.00	0.00	0.00	0.00	0.00	0.00	0.00	0.00	0.00	0.00	0.00	0.00	0.00
di	1.52	1.41	13.34	20.45	9.70	19.14	5.55	32.01	1.86	3.30	0.00	1.39	2.87	0.00
wo	0.00	0.00	0.00	0.00	0.00	2.08	0.00	0.00	0.00	0.00	0.00	0.00	0.00	0.00
hy	20.69	20.90	7.39	1.16	15.55	0.00	24.86	0.00	16.19	14.69	16.16	16.55	17.88	15.52
ol	0.00	0.00	0.00	0.00	0.00	0.00	0.00	2.10	0.00	0.00	0.00	0.00	0.00	0.00
cs	0.00	0.00	0.00	0.00	0.00	0.00	0.00	0.00	0.00	0.00	0.00	0.00	0.00	0.00
mt	1.54	1.55	1.25	1.16	1.82	1.00	2.55	1.83	1.34	1.29	1.24	1.45	1.40	1.24
il	1.77	1.76	2.18	1.83	1.82	1.68	3.01	2.32	1.46	1.45	1.20	1.75	1.57	1.35
ap	0.59	0.59	0.45	0.37	0.28	0.35	0.70	0.23	0.39	0.34	0.34	0.34	0.44	0.52
Tot	99.23	99.22	99.37	99.42	99.08	99.50	98.72	99.07	99.33	99.35	99.38	99.27	99.29	99.38

or calcite. A few accessory opaques are also present as small groundmass phases. Sialic mineral clasts (mainly quartz, up to 1 mm) and holocrystalline fine-grained xenoliths made of feldspar and lesser amphibole, have been also observed in samples F1-17 and F1-18.

Whole rock geochemistry

As previously observed, the investigated Tafresh rock samples generally show the evidence for variable alteration processes, which surely modified the original concentrations of major oxides and trace elements. In order to have a rough idea of the general preservation state, LOI values and CIPW-normative mineralogy have been taken into account, which allowed to make a distinction between (relatively) "fresh" (reported as green symbols in the petrochemical diagrams), "spoiled" (yellow) and "altered" (red) samples.

"Fresh" samples (n=14) have LOI<4.0 wt% (1.80-3.95 wt%), and a SiO_2-oversaturated normative mineralogy that is overall in line with rock petrography (Table 1).

Table 1. ...Continued

sample	F4-11	F1-9	F1-13	F4-15	F3-23	F1-8	F1-29	F1-46	F1-17	F1-18	F2-21	F3-3
geographic coordinates	34°40'N 49°54' E	34°38'N 49°55' E	34°39'N 49°54' E	34°42'N 49°48' E	34°41'N 49°43' E	34°37'N 49°57' E	34°44'N 49°44' E	34°51'N 50°30' E	34°41'N 49°53' E	34°41'N 49°53' E	34°40'N 49°48' E	34°42'N 49°56' E
lithotype	intermediate					evolved			strongly evolved			
preservation	fresh	spoiled				fresh	spoiled		fresh			
SiO_2	58.26	55.56	58.90	52.17	52.89	61.56	60.44	60.27	70.45	70.95	70.11	71.23
TiO_2	0.85	1.22	0.87	1.16	0.90	0.51	0.90	0.51	0.38	0.37	0.33	0.34
Al_2O_3	14.68	16.37	15.21	17.04	16.93	17.68	14.66	16.77	14.49	13.90	12.97	13.52
Fe_2O_{3tot}	7.04	9.51	6.89	8.83	7.29	5.10	7.29	4.33	3.19	3.25	2.54	2.33
MnO	0.12	0.05	0.13	0.12	0.11	0.14	0.11	0.07	0.05	0.05	0.03	0.07
MgO	3.45	3.25	2.55	2.50	2.22	1.59	2.60	2.25	1.20	1.20	1.57	1.08
CaO	5.50	2.98	5.54	9.60	10.25	6.20	2.05	5.38	0.56	1.18	1.26	1.08
Na_2O	3.29	5.69	3.26	2.62	2.95	3.97	5.32	3.81	4.13	3.80	3.11	3.80
K_2O	2.74	0.43	2.53	0.75	0.27	0.50	1.65	2.33	3.84	3.36	3.43	2.68
P_2O_5	0.21	0.18	0.19	0.22	0.17	0.17	0.20	0.20	0.10	0.11	0.06	0.08
LOI	3.65	5.41	4.83	5.91	6.21	3.24	4.24	4.95	1.80	2.30	3.11	2.83
Total	99.79	100.60	100.90	100.90	100.20	100.70	99.46	100.90	100.20	100.50	98.51	99.03
qz	10.79	5.35	13.41	9.10	10.41	19.14	12.14	13.87	27.75	30.77	34.25	35.27
cor	0.00	1.63	0.00	0.00	0.00	0.00	0.92	0.00	2.81	2.17	2.09	2.70
or	16.84	2.67	15.56	4.66	1.70	3.03	10.24	14.35	23.06	20.22	21.24	16.46
ab	28.95	50.55	28.71	23.33	26.56	34.48	47.27	33.61	35.52	32.75	27.58	33.42
an	17.89	14.29	20.19	34.23	34.22	29.71	9.31	22.70	2.16	5.23	6.14	5.03
ne	0.00	0.00	0.00	0.00	0.00	0.00	0.00	0.00	0.00	0.00	0.00	0.00
lc	0.00	0.00	0.00	0.00	0.00	0.00	0.00	0.00	0.00	0.00	0.00	0.00
di	7.50	0.00	5.95	12.11	15.71	0.61	0.00	3.10	0.00	0.00	0.00	0.00
wo	0.00	0.00	0.00	0.00	0.00	0.00	0.00	0.00	0.00	0.00	0.00	0.00
hy	13.93	20.03	12.13	11.30	7.14	10.27	15.85	9.70	6.90	7.01	7.21	5.63
ol	0.00	0.00	0.00	0.00	0.00	0.00	0.00	0.00	0.00	0.00	0.00	0.00
cs	0.00	0.00	0.00	0.00	0.00	0.00	0.00	0.00	0.00	0.00	0.00	0.00
mt	1.26	1.72	1.24	1.60	1.34	0.90	1.32	0.78	0.56	0.57	0.46	0.42
il	1.69	2.44	1.73	2.31	1.82	1.00	1.80	1.01	0.72	0.72	0.65	0.68
ap	0.52	0.45	0.47	0.55	0.43	0.41	0.50	0.49	0.24	0.27	0.15	0.20
Tot	99.37	99.13	99.38	99.20	99.33	99.55	99.34	99.61	99.72	99.71	99.77	99.79

Decreasing mafic minerals (mainly *hypersthene*, from 20.7-21.0 to 13.9-17.9, down to 10.3 vol%) and increasing *quartz* (from 2.53 to 7.60-16.7, up to 19.1 vol%) and sum of sialic minerals (approximately from 73 to 74-81, up to 86 vol%), are indeed observed moving from weakly evolved to intermediate, up to evolved rocks. The strongly evolved rocks have the lowest *hypersthene* (5.63-7.21 vol%) and the highest *quartz* (27.6-35.3 vol%) and sum of sialic minerals (88.5-90.2 vol%), as well as also some CIPW-normative *corundum* (2.09-2.81 vol%), indicative of their peraluminous character.

"Spoiled" samples (n=10) have LOI between 4.0 and 6.5 wt% (4.24-6.21 wt%) and still show some rough consistency between their SiO_2-oversaturated normative mineralogy and observed petrography. Moving from weakly evolved to intermediate and more strongly evolved samples, an increase of *quartz* (from 4.30-8.81 to 5.35-13.4, up to 12.1-13.9 vol%), and of the sum of sialic minerals (from 69.9-75.3 to 71.3-77.9, up to 79.0-84.5 vol%), can be still envisaged. Some major inconsistencies are however evident, e.g.: 1) high *diopside* and *anorthite* of some weakly evolved (summing to >55 vol%) and

Table 2. Trace element concentrations (in ppm) for the investigated rock samples from the Tafresh area with different degree of evolution and preservation (see text). bdl = below detection limits.

sample	F2-12	F2-34	F1-22	F3-24	F4-49	F4-58	F1-33	F1-36	F1-11A	F1-11B	F3-6	F3-13	F4-1
lithotype	weakly evolved								intermediate				
preservation	fresh		spoiled				weathered		fresh				
Rb	45.00	47.00	4.00	9.00	17.00	23.00	13.00	14.00	23.00	53.00	31.00	41.00	20.00
Sr	355.00	357.00	264.00	270.00	229.00	260.00	139.00	203.00	282.00	252.00	374.00	204.00	330.00
Ba	488.00	488.00	147.00	158.00	170.00	181.00	568.00	102.00	405.00	721.00	268.00	329.00	457.00
Cs	1.10	1.20	bdl	bdl	0.60	0.60	0.80	0.70	bdl	0.60	0.60	0.60	bdl
Sc	20.00	20.00	24.00	23.00	30.00	21.00	43.00	35.00	17.00	16.00	14.00	28.00	16.00
V	163.00	165.00	248.00	216.00	284.00	197.00	380.00	257.00	148.00	145.00	119.00	195.00	130.00
Cr	30.00	30.00	50.00	60.00	60.00	60.00	30.00	50.00	bdl	bdl	30.00	bdl	40.00
Co	21.00	21.00	22.00	20.00	16.00	18.00	33.00	33.00	15.00	12.00	11.00	15.00	19.00
Ni	bdl	bdl	30.00	20.00	bdl	30.00	bdl	30.00	bdl	bdl	bdl	bdl	bdl
Cu	20.00	20.00	10.00	30.00	20.00	20.00	220.00	110.00	10.00	100.00	10.00	20.00	10.00
Zn	90.00	90.00	200.00	60.00	80.00	40.00	110.00	80.00	90.00	130.00	80.00	80.00	80.00
Y	30.00	26.00	27.00	22.00	18.00	21.00	36.00	25.00	32.00	28.00	18.00	26.00	25.00
Zr	151.00	150.00	116.00	103.00	69.00	94.00	96.00	69.00	131.00	136.00	107.00	101.00	116.00
Nb	6.00	7.00	5.00	4.00	4.00	3.00	4.00	3.00	7.00	7.00	6.00	5.00	7.00
Hf	3.20	3.20	2.80	2.60	1.70	2.20	2.50	1.70	3.00	3.10	2.40	2.50	2.70
Ta	0.40	0.40	0.30	0.30	0.20	0.20	0.30	0.20	0.40	0.50	0.40	0.40	0.40
La	19.00	19.60	11.70	10.20	9.50	9.10	10.70	6.60	17.30	16.60	15.10	14.40	17.40
Ce	39.40	40.30	25.20	22.10	20.40	20.50	23.80	15.00	35.90	34.90	30.20	30.60	34.7
Pr	4.88	4.88	3.30	2.95	2.64	2.67	3.45	2.16	4.47	4.31	3.63	3.82	4.21
Nd	19.60	20.50	15.00	13.10	11.50	11.80	16.80	10.10	18.10	18.00	13.90	16.00	17.10
Sm	4.70	4.60	3.70	3.50	3.00	3.00	4.80	2.90	4.30	4.20	3.00	3.90	4.00
Eu	1.33	1.32	1.10	0.96	0.88	0.94	1.38	0.93	1.11	1.03	0.84	1.02	1.13
Gd	4.40	4.30	4.00	3.60	2.90	3.20	5.30	3.50	4.20	4.20	2.80	3.70	3.70
Tb	0.80	0.70	0.70	0.60	0.50	0.60	1.00	0.70	0.70	0.70	0.50	0.70	0.60
Dy	4.40	4.50	4.30	3.70	3.30	3.60	6.10	4.10	4.60	4.30	3.00	4.10	4.20
Ho	1.00	0.90	0.80	0.80	0.70	0.70	1.20	0.80	1.00	0.90	0.60	0.90	0.90
Er	2.80	2.70	2.50	2.30	2.00	2.20	3.80	2.60	2.80	2.70	1.80	2.60	2.50
Tm	0.43	0.44	0.41	0.37	0.33	0.36	0.59	0.42	0.48	0.45	0.29	0.41	0.41
Yb	2.90	2.80	2.60	2.30	2.20	2.30	3.80	2.60	3.00	3.10	1.90	2.70	2.70
Lu	0.41	0.41	0.38	0.34	0.30	0.32	0.55	0.37	0.42	0.43	0.27	0.38	0.41
Pb	bdl	bdl	9.00	7.00	bdl	7.0	bdl	bdl	bdl	13.0	bdl	bdl	bdl
Th	4.80	4.80	2.50	2.20	2.30	2.00	1.60	1.80	4.70	4.90	3.90	3.90	3.60
U	1.50	1.50	0.80	0.70	0.70	0.70	0.60	0.50	1.50	1.50	1.30	1.20	1.10
Ga	18.00	19.00	18.00	17.00	18.00	18.00	16.00	15.00	18.00	18.00	17.00	17.00	18.00

intermediate rocks (~45-50 vol%), likely caused by relatively CaO-rich compositions associated to calcite plagues and veins, coupled with very low hypersthene (<1.16 vol%); 2) intermediate sample F1-9 having *corundum* (1.63 vol%), low *quartz* (5.35 vol%) and very high *albite* (50.6 vol%) and *hypersthene* (20.0 vol%); 3) evolved sample F1-29 displaying some *corundum* (0.92 vol%) and very high *albite* (47.3 vol%) and *hypersthene* (15.9 vol%). The relatively high CIPW-normative albite could be related to selective removal of CaO from the

Table 2. ... Continued

sample	F4-10	F4-11	F1-9	F1-13	F4-15	F3-23	F1-8	F1-29	F1-46	F1-17	F1-18	F2-21	F3-3
lithotype	intermediate						evolved			strongly evolved			
preservation	fresh		spoiled				fresh	spoiled		fresh			
Rb	31.00	75.00	13.00	63.00	20.00	4.00	14.00	22.00	65.00	77.00	76.00	76.00	68.00
Sr	317.00	262.00	226.00	229.00	243.00	263.00	317.00	189.00	506.00	137.00	137.00	74.00	112.00
Ba	553.00	496.00	94.00	604.00	196.00	116.00	321.00	383.00	866.00	534.00	489.00	583.00	602.00
Cs	bdl	1.10	0.90	1.60	1.10	1.10	0.50	1.00	2.60	0.70	0.80	0.90	1.30
Sc	12.00	21.00	27.00	22.00	26.00	27.00	7.00	20.00	9.00	9.00	8.00	6.00	7.00
V	94.00	158.00	266.00	167.00	228.00	241.00	51.00	75.00	92.00	51.00	49.00	20.00	22.00
Cr	40.00	80.00	bdl	70.00	50.00	60.00	bdl	bdl	40.00	bdl	bdl	bdl	bdl
Co	12.00	21.00	18.00	18.00	25.00	24.00	6.00	8.00	12.00	5.00	5.00	2.00	2.00
Ni	bdl	30.00	bdl	30.00	20.00	30.00	bdl	bdl	20.00	bdl	bdl	bdl	bdl
Cu	bdl	30.00	10.00	20.00	40.00	40.00	bdl	20.00	20.00	bdl	bdl	bdl	bdl
Zn	100.00	70.00	480.00	80.00	60.00	160.00	60.00	210.00	50.00	50.00	40.00	40.00	50.00
Y	33.00	26.00	29.00	27.00	24.00	23.00	20.00	32.00	8.00	20.00	19.00	22.00	26.00
Zr	169.00	211.00	131.00	221.00	145.00	106.00	103.00	104.00	130.00	128.00	114.00	120.00	135.00
Nb	8.00	10.00	10.00	10.00	11.00	4.00	7.00	5.00	9.00	4.00	5.00	6.00	6.00
Hf	4.10	4.70	3.10	4.80	3.40	2.60	2.50	2.70	3.00	3.30	2.70	3.00	3.10
Ta	0.60	0.80	0.60	0.80	0.70	0.30	0.50	0.40	1.00	0.60	0.50	0.60	0.60
La	22.20	24.40	18.60	25.60	18.30	10.80	15.50	17.10	41.50	18.20	17.90	21.10	21.10
Ce	46.20	49.80	38.50	52.90	37.80	23.70	32.90	38.50	71.00	31.60	32.90	40.40	40.10
Pr	5.68	5.89	4.84	6.05	4.58	3.12	4.04	5.08	7.33	3.68	3.48	4.57	4.35
Nd	23.30	23.70	19.60	24.00	18.90	13.80	16.70	21.60	24.70	13.60	12.60	16.90	16.20
Sm	5.30	5.10	4.60	5.10	4.20	3.50	3.90	5.40	4.10	3.10	2.50	3.50	3.70
Eu	1.33	1.09	1.07	1.18	1.07	0.92	1.18	1.92	0.99	0.72	0.64	0.63	0.77
Gd	4.90	4.50	4.40	4.70	4.00	3.60	3.50	5.40	2.50	3.00	2.30	3.00	3.50
Tb	0.80	0.80	0.80	0.80	0.70	0.60	0.60	0.90	0.30	0.50	0.40	0.50	0.60
Dy	5.30	4.60	5.00	4.70	4.40	3.90	3.40	5.50	1.60	3.10	2.70	3.50	4.00
Ho	1.00	0.90	1.00	1.00	0.90	0.80	0.70	1.10	0.30	0.70	0.60	0.80	0.80
Er	3.20	2.70	3.00	2.90	2.50	2.30	2.10	3.20	0.70	2.00	2.00	2.30	2.50
Tm	0.54	0.44	0.48	0.46	0.39	0.39	0.33	0.52	0.10	0.35	0.33	0.39	0.42
Yb	3.60	2.80	3.10	3.00	2.50	2.50	2.20	3.40	0.60	2.40	2.20	2.70	2.70
Lu	0.56	0.41	0.44	0.42	0.39	0.35	0.32	0.51	0.09	0.37	0.32	0.38	0.40
Pb	6.00	10.00	5.00	8.00	6.00	6.00	bdl	46.00	19.00	bdl	7.00	bdl	bdl
Th	5.00	9.30	4.70	9.80	5.00	2.90	3.10	4.00	22.60	7.00	6.90	8.10	7.90
U	1.60	3.10	1.50	3.10	1.40	1.00	1.10	1.40	10.90	2.1	2.30	2.40	2.40
Ga	19.00	15.00	18.00	16.00	17.00	16.00	17.00	17.00	18.00	14.0	13.00	13.00	13.00

original plagioclase during very low grade metamorphism or normal weathering.

"Altered" samples are represented by two weakly evolved rocks with LOI>9.0 wt% (9.09-9.48 wt%) and some unusual normative mineralogy. Sample F1-33 has relatively high *quartz* and *hypersthene* (respectively 3.57 and 26.9 vol%) and low *orthoclase* (3.04 vol%) and *anorthite* (21.1 vol%), especially if compared to weakly-evolved fresh samples. On the other hand, F1-36 is SiO_2-undersaturated, with *olivine* (2.10 vol%) and some *nepheline* (0.67 vol%), and with *anorthite* and *diopside* summing to ~69 vol%, likely due to the

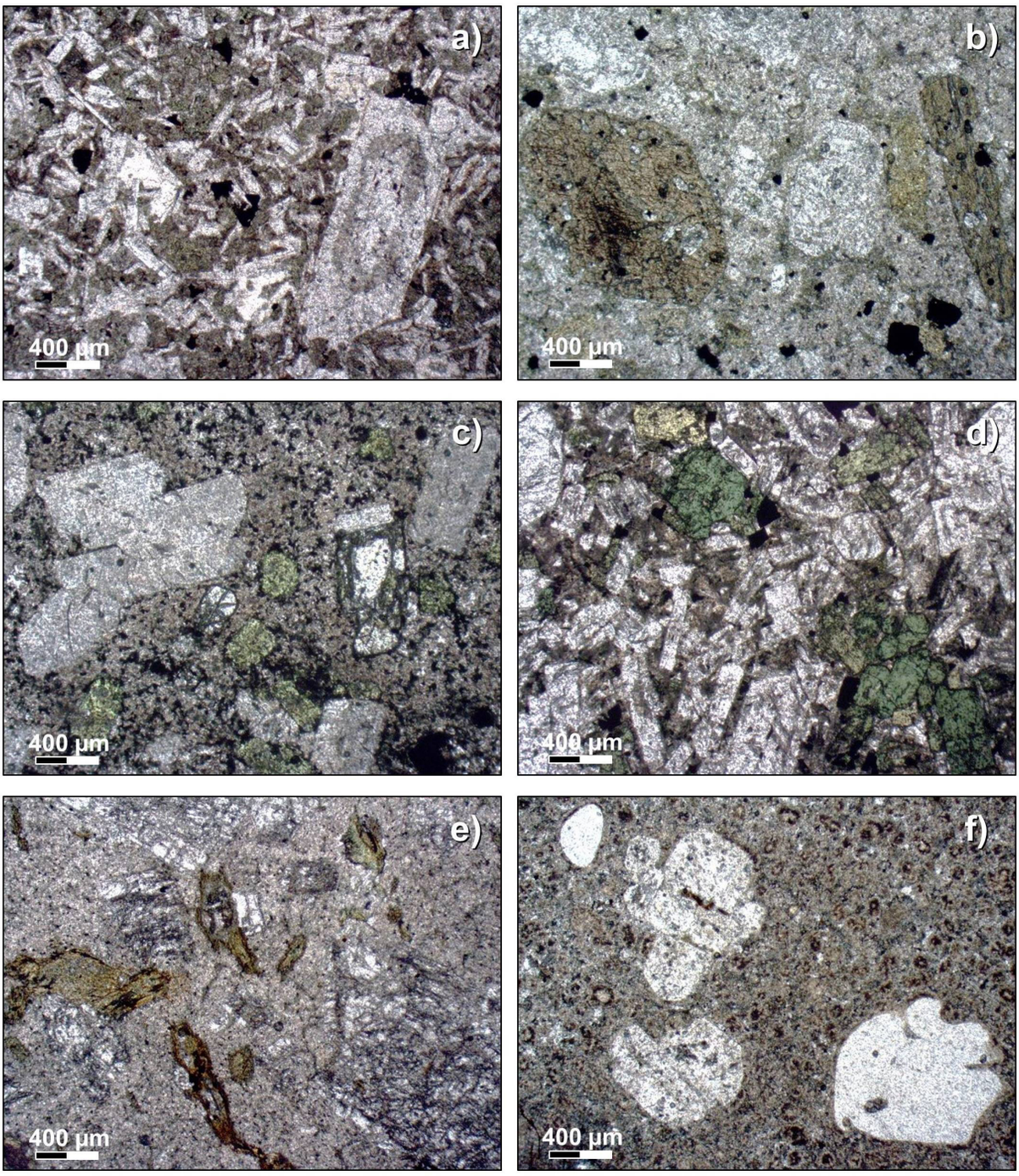

Figure 3. Plane-polarized light photomicrographs of the investigated rock samples from the Tafresh area. a) Weakly evolved rock sample F3-24 showing a holocrystalline intergranular texture consisting of plagioclase and altered ferromagnesian minerals (brownish green); b) intermediate rock sample F3-6 displaying a moderately porphyritic texture with phenocrysts of amphibole (yellow-green) and plagioclase set into an altered (possibly devitrified) groundmass; c) intermediate rock sample F4-11 showing a moderately porphyritic texture with phenocrysts of altered plagioclase (dusty-looking), amphibole (light green) and clinopyroxene (colourless, e.g., centre right) set into an altered microcrystalline groundmass; d) intermediate rock sample F4-15 with a holocrystalline hypidiomorphic texture essentially made of plagioclase and amphibole crystals; e) evolved rock sample F1-8 showing a weakly porphyritic texture with phenocrysts of feldspars and amphibole set into an altered (devitrified?) groundmass; f) strongly evolved rock sample F3-3 displaying a moderately porphyritic texture with phenocrysts of feldspars and quartz (e.g., embayed crystal at the lower right) set into a devitrified groundmass.

presence of secondary calcite veins, lowering the absolute SiO_2 whole-rock content. The high CIPW-normative hypersthene could be related to the common presence of serpentine-group minerals.

Well bearing in mind the above observations, the alteration effects on changing the composition of the investigated samples are evaluated through a comparison with literature data from the same area and from the entire UDMA. The latter group of data was restricted to rocks with "orogenic" affinity and filtered by removing analyses likely suffering from intense alteration, i.e., those with LOI>4.0 wt% and with sum of major element oxides <98.0 wt% or >102.0 wt%. Data for which LOI values are not reported were cautiously discarded as well.

Classification and serial affinity

The investigated Tafresh rocks have been categorized using different classification schemes. Based on the TAS classification, Tafresh samples plot in the subalkaline field, with rock compositions being largely consistent with petrography, regardless of the degree of alteration (Figure 4a). The weakly evolved rocks are mainly basaltic andesites (SiO_2=53.7-55.6 wt%; Na_2O+K_2O=3.24-5.67 wt%), with one altered sample plotting in the basalt field with the lowest SiO_2 (49.0 wt%) and sum of alkalis (3.03 wt%). Intermediate rock samples are mostly andesites with 57.8-61.3 wt% SiO_2 and 4.48-6.43 wt% Na_2O+K_2O, except for two spoiled samples and one fresh sample falling in the field of basaltic andesites (the latter almost at the boundary with the andesite field) and one spoiled sample falling just above the andesite-trachyandesite divide. Evolved rocks are quite homogeneous in terms of SiO_2 (62.8-63.5 wt%), but display some larger variability in the sum of alkalis (4.59-7.32 wt%), with two samples straddling the boundary between andesite and dacite and the alkali-richest spoiled sample falling in the latite field. Finally, the fresh strongly evolved rocks are all classified as rhyolites, with SiO_2 ranging from 71.6 and 74.0 wt% and sum of alkalis in the range of 6.74-8.10 wt%.

In order to compare the investigated Tafresh samples with those from the existing literature, the latter have been distinguished based on their main parageneses into: 1) "basaltic" (pl+cpx±ol), 2) "andesitic" (pl+amph±cpx), 3) "dacitic" (feld+amph±bt) and 4) rhyolitic (feld+qtz). Although there is an overall consistency between literature and present samples in terms of general degree of rock evolution and SiO_2 content, literature samples display some major variation for the sum of alkalis, which spans a very wide compositional spectrum for all the lithotypes, except the rhyolitic ones. Notably, an overall good consistency is also evidenced with literature "orogenic" rocks from the UDMA. Worth noting, UDMA rocks also include dacitic compositions in the SiO_2 range of 64.0-70.0 wt% (not represented in Tafresh rocks), as well as a few samples with high sum of alkalis, possibly belonging to a shoshonitic rock series.

Similar observations arise from the K_2O vs SiO_2 diagram of Figure 4b, where the investigated Tafresh rocks define mostly a medium-K to high-K calcalkaline series, with only a few K_2O-poor rock samples (0.29-0.51 wt%) falling in the field for low-K tholeiitic rock series. Literature Tafresh samples are still very scattered due to their extremely variable K_2O contents, but they mainly lie in the fields for medium-K and high-K rock series. Finally, also literature UDMA rocks with "orogenic" affinity belong mainly to the medium- and high-K series, although there are also some samples with shoshonitic serial affinity and a few K_2O-poor outliers.

Additional classification plots, specifically thought for altered samples using immobile elements, are also taken into account in Figure 5. The Zr/TiO_2 vs Nb/Y plot again confirms the subalkaline serial affinity and the overall consistency between petrographic types and chemical compositions for the Tafresh samples from both this work and the existing literature, being classifiable mostly as andesite and dacite/rhyodacite. Similar considerations can be made for in the Th vs Co diagram, where the investigated Tafresh samples mostly plot in the calcalkaline series field. Literature UDMA samples are again largely consistent with Tafresh samples, defining a full calcalkaline rock series and including the most evolved compositions with shoshonitic affinity.

Major and trace elements variations

The investigated Tafresh samples define some overall coherent differentiation trends in major element binary variation plots (Figure 6), which are especially evident if only relatively fresh samples are taken into account. With increasing silica contents, a quite regular decrease is observed for TiO_2, Al_2O_3, Fe_2O_{3tot}, MgO and CaO, whereas K_2O increase, and Na_2O and P_2O_5 faintly increase up to the evolved rock samples and then decrease in the strongly evolved ones. Some major scattering is observed for spoiled and altered samples, mostly in some weakly evolved rocks with unusually high (19.7-20.4 wt%) or low (15.0 wt%) Al_2O_3, high Fe_2O_{3tot} (14.8 wt%), low MgO (1.23-2.54 wt%) and high CaO (11.2-15.2 wt%, likely due to secondary calcite). Tafresh literature samples, although roughly in line with the above differentiation trends, display some more evident data scattering for most of the major elements. The observed trends are on the whole in line with those depicted by UDMA "orogenic" rocks.

Binary variation diagrams for trace elements (Figure 7) are remarkably more scattered. A general decreasing trend can be envisaged for Sc and V only, well consistent with the trend defined by the UDMA "orogenic" rocks. On the

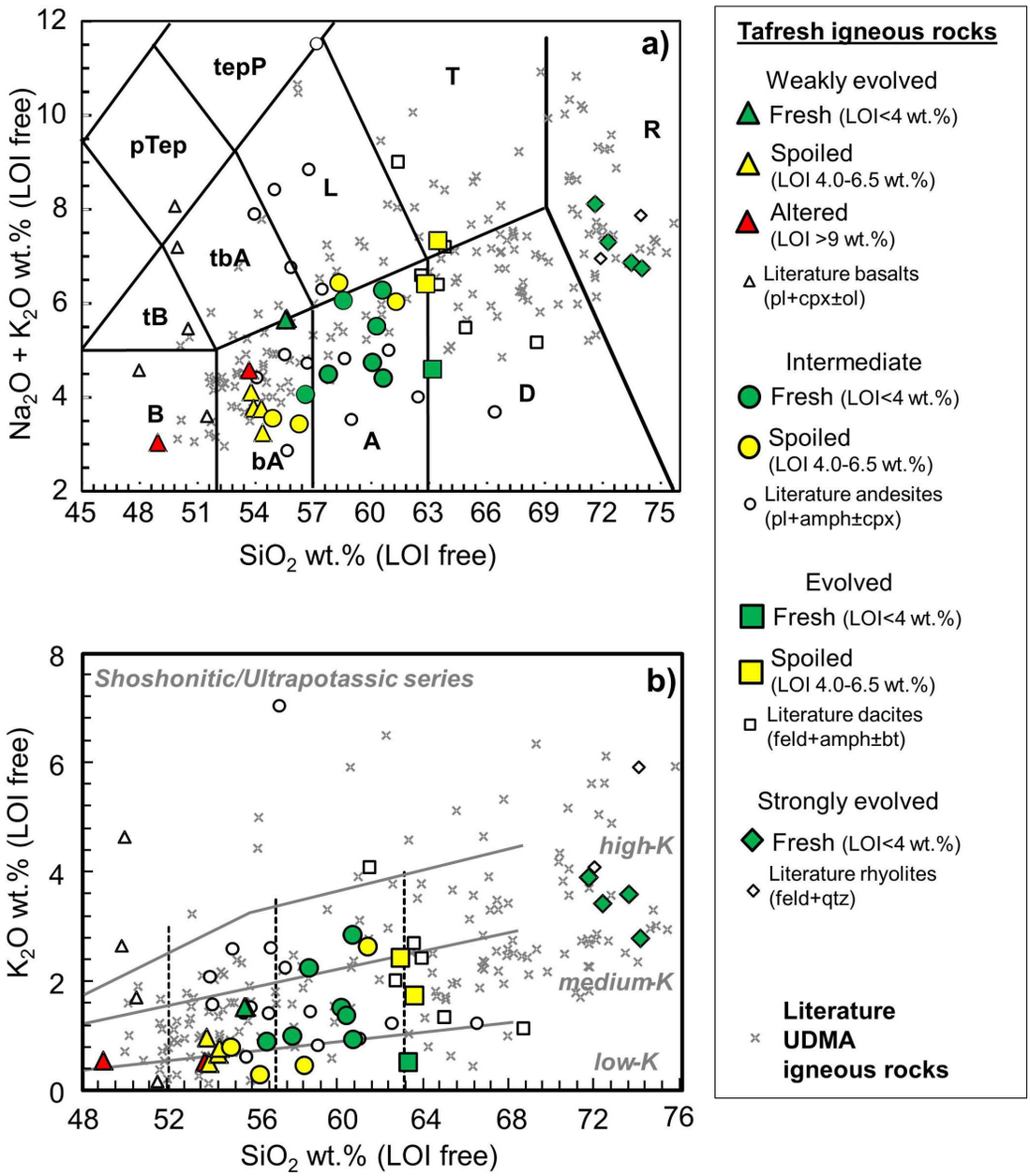

Figure 4. a) TAS (Total Alkali vs Silica) and b) K_2O vs SiO_2 (Le Maitre, 2002) classification diagrams for the Tafresh area rock samples from this work and from the available literature (Ghorbani and Bezenjani, 2011; Khademi et al., 2019). Selected literature data for the UDMA rocks with "orogenic" affinity (Boccaletti et al., 1977; Riou et al., 1981; Jahangiri, 2007; Omrani et al., 2008; Sherafat et al., 2012; Maanijou et al., 2013; Yeganehfar et al., 2013; Azizi et al., 2014; Honarmand et al., 2014) are also reported for comparison (see text for further details). Abbreviations for rock names (in black): A = andesite; B = basalt; bA = basaltic andesite; D = dacite; L = latite; P = phonolite; pTep = phonotephrite; R = rhyolite; T = trachyte; tB = trachybasalt; tbA = trachybasaltic andesite; tepP = tephriphonolite.

other hand, Rb, Sr (very scattered), Ba, Zr and Nb define a trend of broad increase with increasing differentiation, while Y is mostly constant except from a few outliers. Among the evolved rocks, sample F1-46 generally plots close to a group of literature dacitic samples due to its relatively high Sr (506 ppm), Ba (866 ppm), Th (23 ppm), Cr and Ni (respectively 40 and 20 ppm; Figure S1), and low Y (8 ppm). It is interesting to note that many incompatible trace elements remain roughly constant or even record some slight decrease in the transition from the evolved to the strongly evolved samples (e.g., Sr, Ba, Y, Zr and Nb).

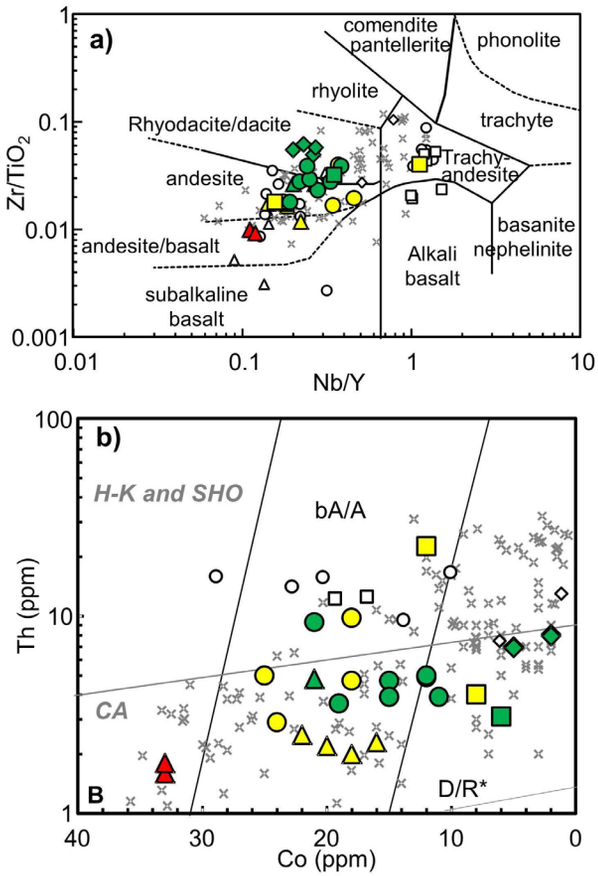

Figure 5. a) Zr/TiO_2 vs Nb/Y (Winchester and Floyd, 1977) and b) Th vs Co (Hastie et al., 2007) classification diagrams for the Tafresh area rock samples (this work and literature data) and for selected literature data for the UDMA rocks with "orogenic" affinity. Symbols and sources of bibliographic data as in Figure 4. Abbreviations for rock names (in black): B = basalt; bA = basaltic andesite; D/R = dacite/rhyolite (* indicates that latites and trachytes also fall in these fields). Abbreviations for rock series (in grey): CA = calcalkaline; H-K = high-K calcalkaline; SHO = shoshonitic.

Chondrite-normalized Rare Earth Elements patterns

The Rare Earth Elements (REE) concentrations of the investigated Tafresh rocks have been normalized to CI chondrite average estimate in Figure 8. The patterns for the least evolved samples are slightly enriched in Light REE (LREE; La_N/Lu_N 1.91-5.12, N for normalized abundances) and nearly flat in Middle and Heavy REE (MREE and HREE; Dy_N/Lu_N 1.07-1.13), with normalized abundances for the most enriched REE at 28-83 times chondrite abundances (xCI; Figure 8a). Some small troughs at Eu are also observed, with Eu/Eu* [$Eu_N/(Sm_N*Gd_N)^{0.5}$] in the range of 0.83-0.93. No substantial differences can be observed in rocks with different degree of preservation, with the slightly more enriched patterns of the relatively fresh samples possibly only reflecting their slightly more evolved character. Literature data for the Tafresh area and UDMA "orogenic" rocks with similar degrees of differentiation are in line with the present data, although three "anomalous" basaltic samples from Tafresh are also evidenced (samples T7, T19 and T2; Figure 8a). Intermediate samples display very homogeneous patterns that are on the whole similar to the weakly evolved ones, reaching also slightly more enriched compositions with the highest normalized abundances in the range of 46-103 xCI, La_N/Lu_N 3.31-6.53, Dy_N/Lu_N 0.95-1.14 and Eu/Eu* =0.70-0.90 (Figure 8b). Tafresh andesitic rocks from the literature are mostly overlapping, although some slightly less enriched samples are also present. As for the evolved samples, two rocks display nearly identical patterns that are very similar to those for the intermediate rocks, (Figure 8c). On the other hand, the spoiled sample F1-46 has not only the highest LREE (up to ~175 xCI), but also strong LREE/HREE (La_N/Lu_N 49.4), LREE/MREE (La_N/Sm_N 6.53) and even MREE/HREE (Dy_N/Lu_N 1.78), coupled with Eu/Eu*=0.95. The pattern of this sample matches perfectly with the available literature data for Tafresh dacitic rocks.

Finally, the strongly evolved rocks have very homogeneous and peculiar REE patterns with no counterparts in the Tafresh literature. Indeed, these display slight LREE/HREE enrichment (La_N/Lu_N 5.27-5.99), MREE/HREE depletion (Dy_N/Lu_N 0.84-0.92, except for one sample with 1.00), strong Eu troughs (Eu/Eu*=0.59-0.82), and normalized abundances up to 76-89 xCI (Figure 8c).

Primitive mantle-normalized multielemental patterns

In primitive mantle-normalized (hereafter PM-normalized)multielemental diagrams, the Tafresh least evolved rocks display some spiky patterns with major scattering for the most incompatible elements. This is likely due to their mobility in aqueous fluids, as observable from the differences of the patterns for spoiled and altered samples (Figure 9a). The remaining least incompatible elements show significantly lower scattering, with marked enrichment in LILE (Large Ion Lithophile Elements) with respect to the HFSE (High Field Strength Elements), peaks at K and Pb, as well as troughs at Nb, Ta and Ti. These strongly resemble the patterns for average upper crustal rocks (e.g., Rudnick and Gao, 2014), the average composition of the Global Subducting Sediments (GLOSS; Plank, 2014), and the typical subduction-related magmas (e.g., Zheng, 2019). Literature rocks from the Tafresh area and the UDMA with similar degree of differentiation show similar patterns, again excluding the three outliers, previously defined as "anomalous" basaltic samples (see previous section). As observed for CI-normalized

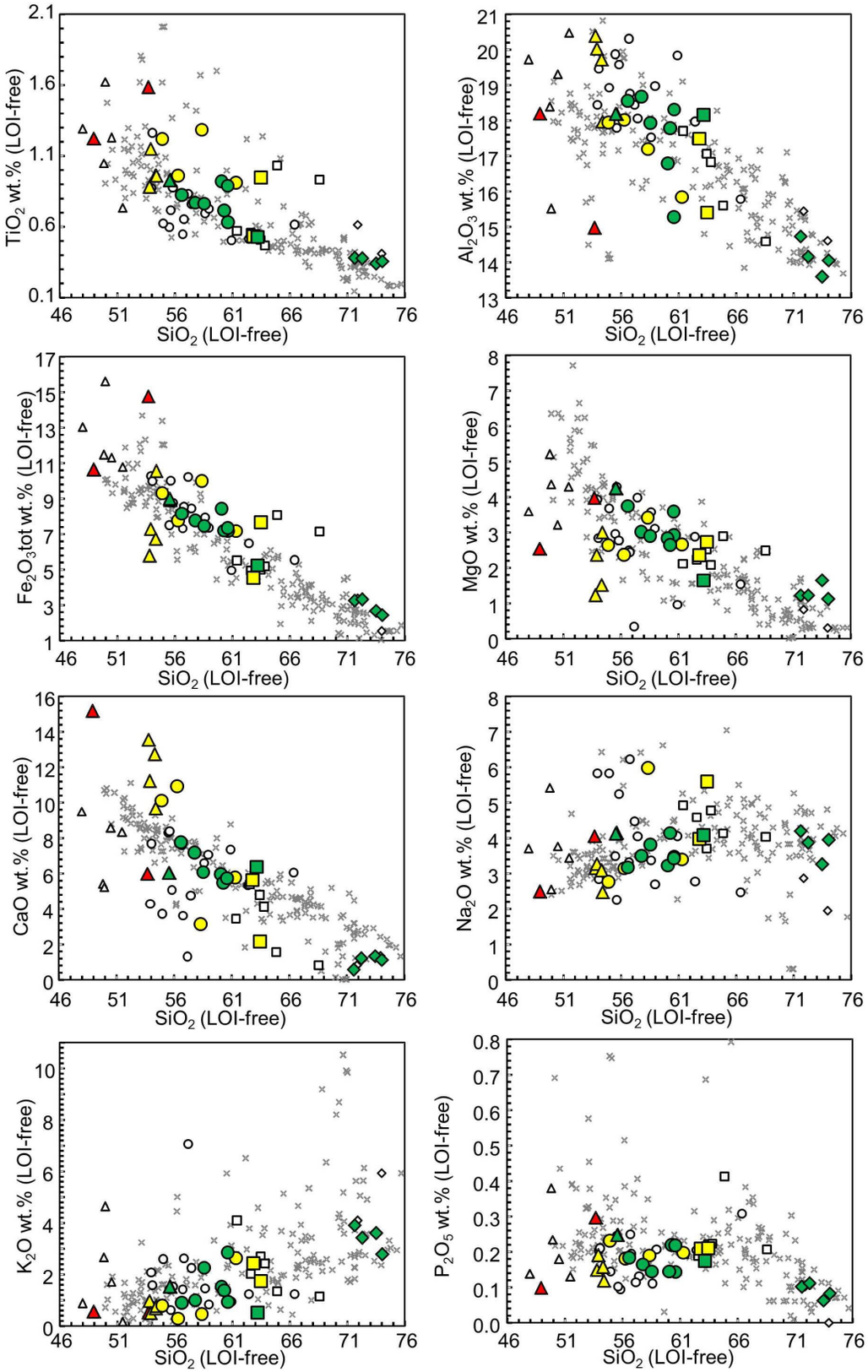

Figure 6. Major elements vs SiO_2 variation diagrams for the Tafresh area rock samples (this work and literature) and for selected literature data for the UDMA rocks with "orogenic" affinity. Symbols and sources of bibliographic data as in Figure 4.

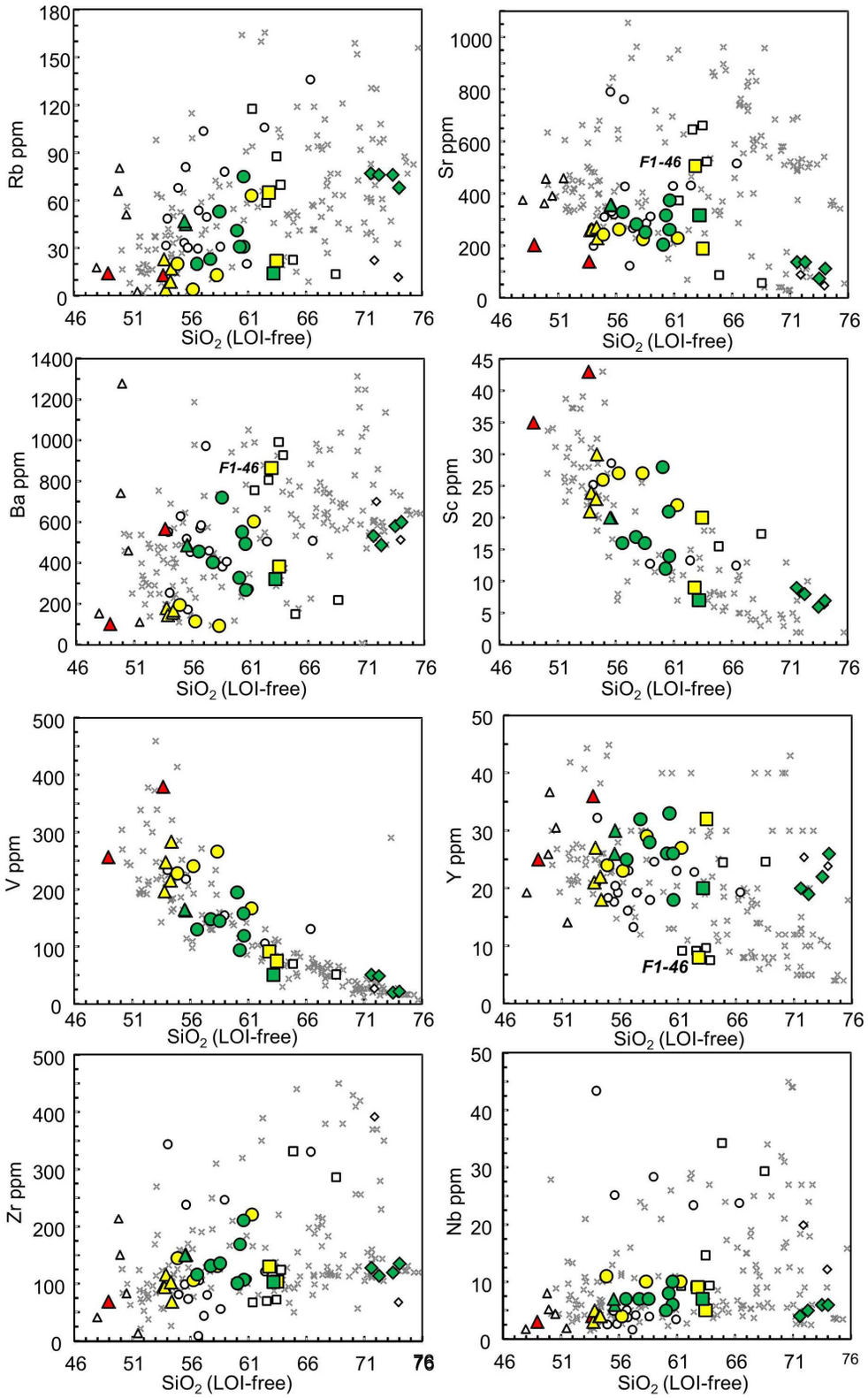

Figure 7. Selected trace elements vs SiO_2 variation diagrams for the Tafresh area rock samples (this work and literature) and for selected literature data for the UDMA rocks with "orogenic" affinity. Variation diagrams for the remaining trace elements are reported in Figure S1. A highlight on sample F1-46 is provided where its composition is significantly deviating from that of the other evolved samples. Symbols and sources of bibliographic data as in Figure 4.

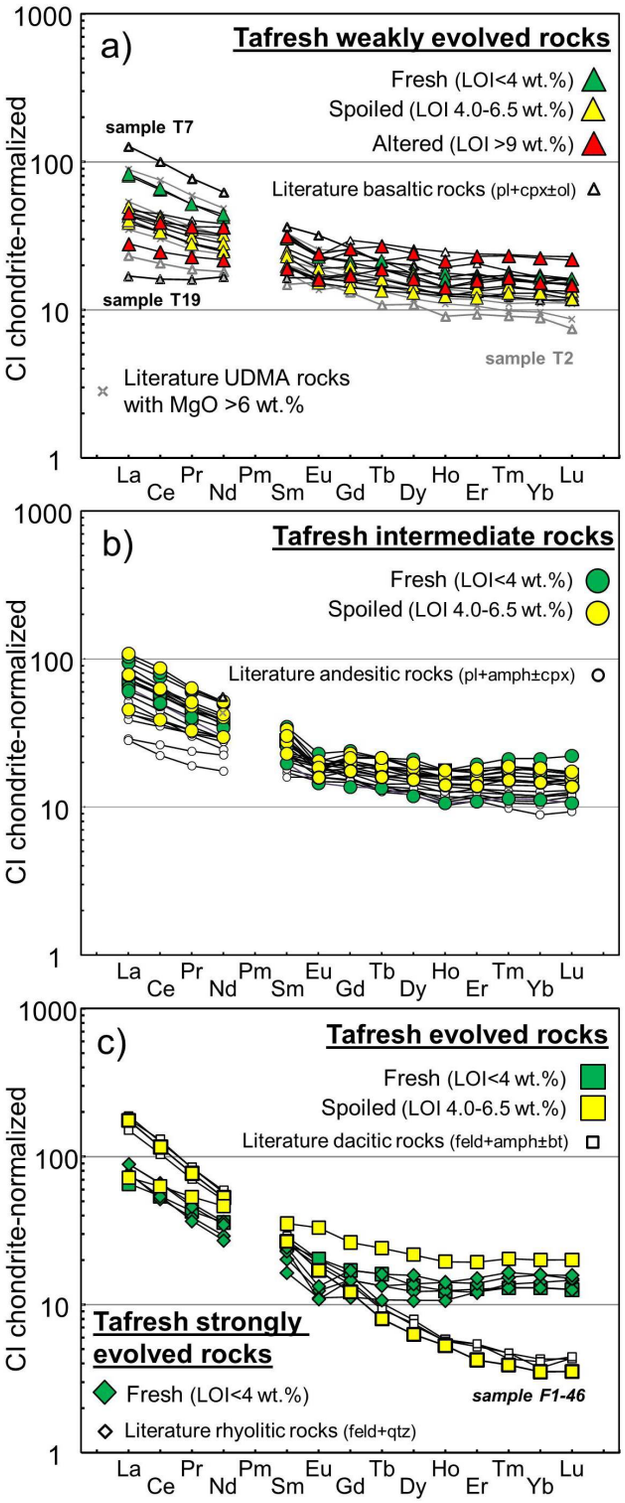

Figure 8. Chondrite-normalized (King et al., 2020) REE plots for the Tafresh area rock samples of a) weakly evolved (plus literature "basaltic", with a highlight on the "anomalous" samples T2, T7 and T19; see text for further details), b) intermediate (plus literature "andesitic") and c) evolved (plus literature "dacitic"; a highlight on sample F1-46 is also provided) and strongly evolved compositions. In a) literature data for weakly evolved (MgO >6 wt%) UDMA rocks with "orogenic" affinity are also reported. Sources of bibliographic data as in Figure 4.

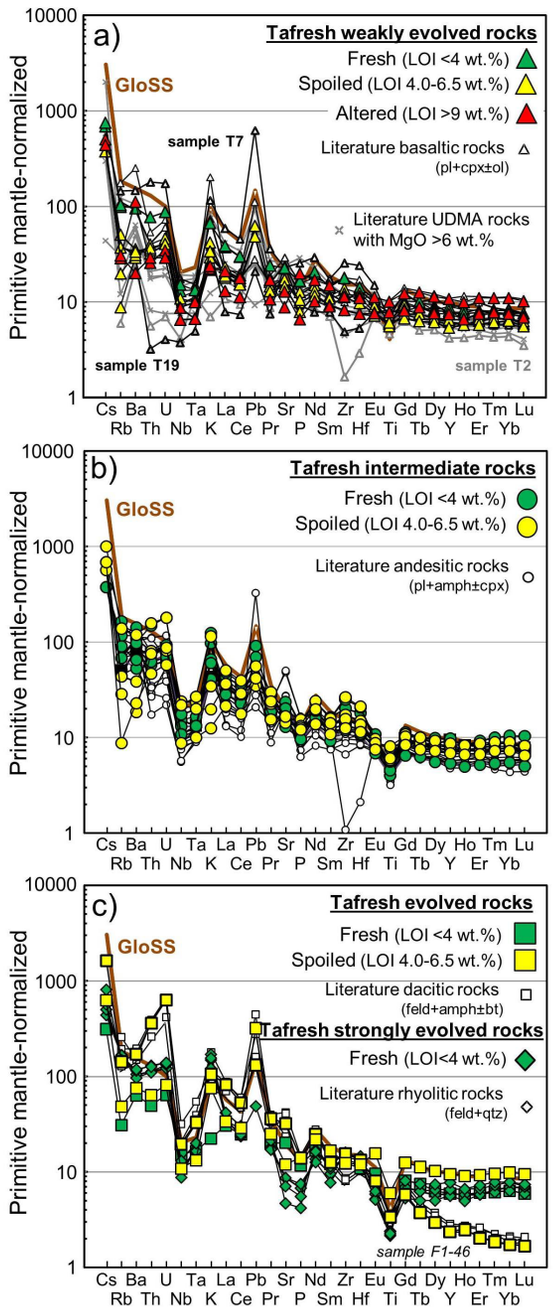

Figure 9. Primitive mantle-normalized (Lyubetskaya and Korenaga, 2007) multielemental plots for the Tafresh area samples of a) weakly evolved (plus literature "basaltic", with a highlight on the "anomalous" samples T2, T7 and T19; see text for further details), b) intermediate (plus literature "andesitic") and c) evolved (plus literature "dacitic"; a highlight on sample F1-46 is also provided) and strongly evolved compositions. The pattern for the estimated composition of Global Subducting Sediments (GLOSS; Plank, 2014) is included for comparison. In a) literature data for weakly evolved (MgO >6 wt%) UDMA rocks with "orogenic" affinity are also reported. Sources of bibliographic data as in Figure 4.

patterns, PM-normalized patterns for the intermediate rocks are extremely homogeneous (except for some scattering in the most incompatible fluid-mobile elements; Figure 9b). Overall, a strong similarity can be envisaged with patterns for the weakly evolved rocks, although some general displacement to slightly higher abundances and a faint to moderate peak at Zr-Hf are also observed. Tafresh andesitic rocks from the literature are perfectly in line with these patterns, with some few exceptions (e.g., higher K, Pb peak and Zr-Hf depletion). Evolved Tafresh rocks define two distinctive groups of rocks with peculiar PM-normalized patterns, both characterized by the overall LILE/HFSE enrichment observed for the weakly evolved and intermediate samples (Figure 9c). Sample F1-46 and dacitic rocks from the literature have the strongest LILE enrichment of the entire dataset, coupled with a marked depletion for MREE, Y and HREE and a small but evident peak at Sr. On the other hand, the remaining two evolved samples display a pattern virtually identical to that of the most enriched intermediate rocks. The patterns for the strongly evolved Tafresh rocks is also very similar, except for having smaller Pb peaks and a marked depletion at Sr and P.

DISCUSSION

The investigated rocks from the Tafresh area include a relatively large variety of lithotypes, covering the entire compositional spectrum for a typical subduction-related "orogenic" subalkaline to mildly alkaline series. Intermediate compositions are by far the most represented, with much rarer weakly evolved and evolved lithotypes and some strongly evolved leucocratic compositions. Field and petrographic evidence suggest that the outcropping rocks were emplaced not only in a "volcanic" environment, but also at various depths within the crust (e.g., textures including both porphyritic, possibly with glassy groundmass, as well as holocrystalline medium- to coarse-grained hypidiomorphic and fine- to medium-grained intergranular "dolerite-like" types). Notwithstanding the overall poor preservation due the alteration processes, geochemical data define on the whole some generally coherent trends that, at least at a first level of investigation, support the existence of some genetic relation linking them. However, several observations suggest that additional processes other than simple closed-system fractional crystallization were also active: 1) presence of possibly xenocrystic large crystals in textural disequilibrium; 2) presence of large amphibole oikocrysts (with plagioclase inclusions), likely cumulitic in origin; 3) presence of xenoliths in the strongly evolved rocks; 4) observation of some sparse "anomalous" geochemical features (e.g., sample F1-46, incompatible element contents not linearly increasing with the degree of

differentiation) that do not seem to be related to alteration processes only.

It is therefore evident that reconstructing the petrogenetic processes operating together in the Tafresh area could be a particularly hard task, with numerous processes possibly acting together and thus overlapping their effects. In the following sections, a qualitative/semi-quantitative treatment of such processes in tentatively undertaken, with the aim of shedding some light on the petrogenesis of the outcropping rocks and making some inferences in the larger framework of the geodynamic evolution of the UDMA.

Magmatic lineages and differentiation processes in the Tafresh area

Assessing whether the investigated Tafresh rocks represent a single liquid line of descent or rather include two or more independent magmatic lineages is greatly complicated by the aforementioned bad preservation state that generally characterizes them. Alteration processes not only variably (and rather unpredictably) modified original rock compositions, but also significantly obscured the primary paragenesis, thus making also the proposed lithological distinction not completely reliable. Consequently, the recognized rock types should not be considered as coherent, homogeneous groupings, and some overlap between rocks with similar degrees of evolution should be expected.

Bearing this in mind, a quite regular evolutionary trend seems to be recognizable from the weakly evolved to the intermediate rocks based on both variation and CI- and PM-normalized diagrams. The main fractionating phases are likely represented by ferromagnesian minerals (mostly clinopyroxene and olivine) and plagioclase, then followed by an assemblage made up of plagioclase, amphibole and minor clinopyroxene (e.g., CaO being roughly constant up to ~53 wt% SiO_2, then firmly decreasing), in broad good accordance with petrography. This trend possibly extends also to the evolved rock samples (with a decrease in fractionating amphibole and the onset of alkali feldspar fractionation), with the only exception of sample F1-46, which has been observed to display some rather "anomalous" features. This sample, collected in a different location, ~20 km N from the main sampling area, is characterized by high Sr, low Y, coupled with high LREE/HREE, LREE/MREE and MREE/HREE ratios, typical of adakitic magmas (as well as for tonalite-trondhjemite-granodiorite "TTG" suites, widespread during the Archean; e.g., Martin et al. 2005; Palin et al., 2016). The occurrence of such compositions is widely recognized in the literature for both the Tafresh area ("dacitic" rocks; Ghorbani and Bezenjani, 2011; Ghorbani et al., 2014) and the entire UDMA (Jahangiri, 2007; Khodami et al., 2009; Omrani et al., 2008; Sherafat et al., 2012; Yeganehfar et al., 2013; Azizi et al., 2014, 2019; Ghorbani et al., 2014; Pang et al., 2016; Alirezaei et al., 2017; Torkian et al., 2018; Kheirkhah et al., 2020). The genesis of these peculiar rock compositions will be considered in a following section.

Numerous lines of evidence suggest that Tafresh strongly evolved rocks are not genetically linked with the main products cropping out in the area. The large compositional gap of ~5 wt% SiO_2 separating them from the evolved rocks (not taking into account the rocks with adakitic signature) suggests the absence of a continuous spectrum of magma compositions. In addition, the transition from the two lithotypes is not characterized by a clear decrease in elements that are strongly partitioned in feldspars such as Na_2O, K_2O and Ba (although there is a decrease in Eu and, less evident, in Sr). For this reason, a focus on this group of rocks is provided in a further following section.

We therefore conclude that most of the Tafresh rocks likely represent the products of a single liquid line of descent with the typical features of a magma series generated from subduction-modified mantle sources. These include: 1) Al-rich, Fe-poor whole rock compositions, likely reflecting water-rich and oxidized source regions; 2) plagioclase-phyric, olivine-poor hydrous mineral-bearing paragenesis; 3) LILE-enriched and HFSE-depleted PM-normalized patterns; 4) predominance of intermediate "andesitic" lithotypes; 5) scarcity (or even complete lack) of primitive lithotypes. Based on the latter, it is clear that no specific inferences can be made on the nature of the mantle source(s), which can be only approximately assumed to be represented by a metasomatized peridotite in the spinel stability field (as indicated by the flat HREE PM-normalized pattern of the least evolved Tafresh rocks). Primitive melts were likely hydrous, as also confirmed by presence of abundant amphibole in the intermediate rocks, which also suggests that differentiation processes occurred at shallow to moderate depths. Following experimental results for "orogenic" magmas, the observed crystallisation sequence with plagioclase appearing on the liquidus before amphibole requires that primitive melts were not particularly rich in H_2O [<4.5 wt%, based on the phase diagrams of Melekhova et al. (2015) for a high-MgO basalt] and that these evolved at ~4 kbar [see the phase diagram of Pichavant et al. (2002) for a basaltic andesite with ~6 wt% H_2O].

Genesis of the strongly evolved rocks from the Tafresh area

The genesis of strongly evolved rocks is likely unrelated to that of the main magmatic suite emplaced in the Tafresh area. The frankly peraluminous nature of such rocks [A/CNK=Al/(Ca+Na+K)=1.16-1.22, compared to

the 1.22-1.45 range in literature samples] makes them more akin to melts generated from crustal anatexis of metaigneous or metasedimentary protoliths (e.g., I- and S-type granites; e.g., Clemens et al., 2011; Chappell et al., 2012), rather than to typically highly fractionated melts from metaluminous parental magma (e.g., M-type granites). The latter could be also weakly peraluminous, if substantial fractionation of metaluminous phases such amphibole occurs (Chappell et al., 2012), but this does not seem the case of Tafresh strongly evolved rocks, in which amphibole remains as a subordinate phase. This is also supported by the lack of a marked MREE depletion that would be expected if significant amphibole fractionation had occurred, given the high $^{amphibole/melt}D_{MREE}$ (e.g., Nandedkar et al., 2016). Therefore, the Tafresh strongly evolved rocks can be related either to partial melting of Al-rich (meta-) igneous or sedimentary rocks from the local crust, (e.g., the Neoproterozoic and Paleozoic and Mesozoic basement rocks; Bagheri and Stampfli, 2008; Horton et al., 2008) or to interaction of metaluminous evolved magmas with Al-rich crustal rocks.

The first hypothesis (crustal anatexis) is somewhat more in line with the leucocratic nature of such rocks, indicating a composition that is possibly close to that of the granite minimum in the petrogeny's residua system. However, a discrimination between a meta-igneous or meta-sedimentary source seems not so straightforward, as high-SiO_2 melts from these two sources share many similarities (e.g., Chappell, 1999; Chappell and White, 2001; Clemens and Stevens, 2012; Jagoutz and Klein, 2018). The very low CaO/FeO (0.61-0.86, plus one literature sample with 1.18) and low Sr (47-137 ppm) of Tafresh strongly evolved rocks is more consistent with a sedimentary source. On the other hand, the quite regular major and trace element variation trends and the linear decline of P_2O_5 at increasing SiO_2 would rather suggest a metaigneous source rock. In addition, other geochemical parameters reveal some evident differences between strongly evolved samples from this study and the two literature samples from Khademi et al. (2019). The latter have low Na_2O (1.94-2.86 wt%) and Al_2O_3/TiO_2 (25.2-35.8), very low Rb/Sr (0.25) and Rb/Ba (0.02-0.03) and relatively high CaO/Na_2O (0.29-0.68), suggestive of a (relatively) plagioclase-rich, clay-poor source (e.g., Sylvester, 1998). On the other hand, the strongly evolved Tafresh rocks reported here have relatively high Na_2O (3.26-4.20 wt%), Rb/Sr (0.55-1.03) and Rb/Ba (0.11-0.16), plus slightly higher Al_2O_3/TiO_2 and generally lower CaO/Na_2O (0.14-0.41), more in line with a meta-pelitic source rock. On such basis, it could be tentatively proposed that Tafresh strongly evolved rocks originated from the melting of a heterogeneous metasedimentary source consisting of both meta-pelitic and (relatively) plagioclase-rich meta-greywacke components.

As an alternative, a process of interaction between a metaluminous melt with upper crustal Si-Al-rich lithologies is also viable, provided that some phase in which MREE are preferentially partitioned is simultaneously fractionating, in order to produce the observed slight MREE depletion. This could be obtained through both some limited amphibole fractionation (see above), or fractionation of accessory phases such as apatite and titanite, which also preferentially host MREE with respect to LREE and HREE (e.g., Prowatke and Klemme, 2006 a,b).

Genesis of the Tafresh area evolved rocks with adakitic geochemical fingerprint

As highlighted in a previous section, Tafresh evolved rocks include products resembling adakitic compositions that deserve additional considerations. The supposed adakitic signature can reflect primary features or rather it could be acquired due to alteration processes. For this reason, we decided to compare their overall geochemistry with those of adakitic/TTG magmas as reported by Martin et al. (2005). With respect to the latter, Tafresh rocks have: 1) slightly lower SiO_2 (61.4-63.8 wt%, vs mostly >64 wt%); 2) relatively low Na_2O (i.e., 3.7-4.9 wt% vs 3.0-7.0 wt%); 3) higher K_2O/Na_2O (0.4-0.8 vs <0.5); 4) higher sum of ferromagnesian elements (Fe_2O_{3tot}+MgO+MnO+TiO_2 =7.5-8.3 wt% vs <5.0 wt%); 5) La_N/Yb_N only moderately high (34-49 vs up to 150). Finally, when plotted in the classical adakite discrimination diagrams (Figure 10) these rocks plot well within the field for adakitic melts (along with numerous other UDMA occurrences from the existing literature). It is therefore concluded that such evolved rocks should be actually considered as adakites, and some of the above small deviations from the typical adakite geochemical fingerprint might be due to secondary mobilization of some major elements during alteration.

Adakitic melts are classically interpreted to represent the product of slab melting in active and hot subduction zones, with variable extents of interaction with the peridotitic matrix (e.g., Defant and Drummond, 1990; Drummond and Defant, 1990; Martin et al., 2005; Moyen, 2009; Castillo, 2012; Ma et al., 2012; Breitfeld et al., 2019; Liu et al., 2019). Adakite occurrences have also been reported for subduction-unrelated geological settings, supporting alternative models involving, e.g., melting of the lower crust (e.g., Chung et al., 2003; Wang et al., 2006; Ma et al., 2012). Finally, more recent models proposed to produce the high Sr/Y and La/Yb "adakitic" signature (e.g., Macpherson et al., 2006; Rodríguez et al., 2007; Kamei et al., 2009; Moyen, 2009; Castillo, 2012; Ribeiro et al., 2016; Bellver-Baca et al., 2020), point to different mechanisms, including melting of a high

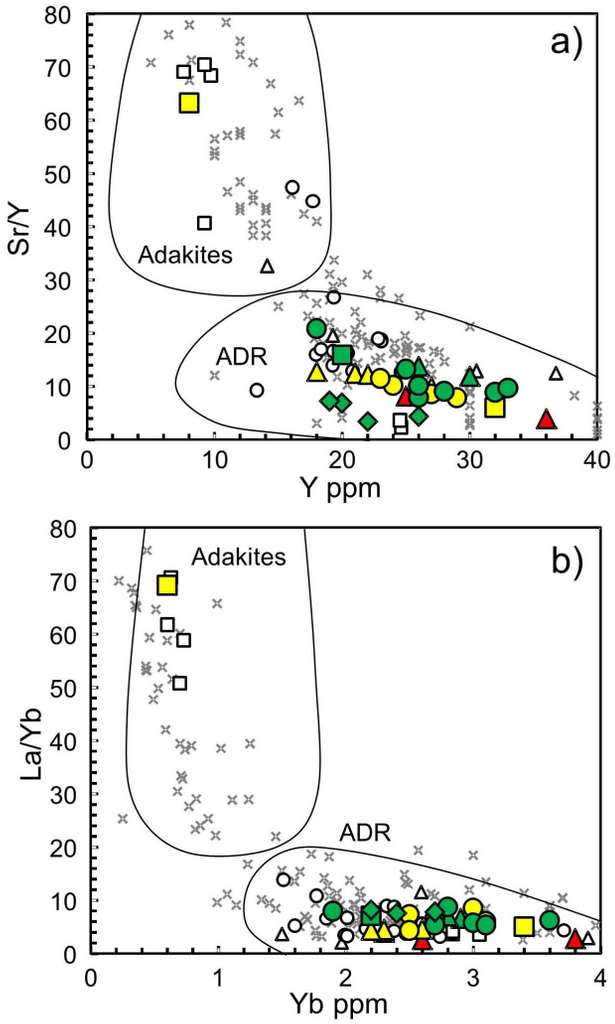

Figure 10. a) Sr/Y vs Y and b) La/Yb vs Yb diagrams [Drummond and Defant (1990), modified after Richards and Kerrich (2007)], used to distinguish adakites from "normal" arc andesite, dacite and rhyolite (ADR), for the Tafresh area samples (this work and literature) and for selected literature data for the UDMA rocks with "orogenic" affinity. Symbols and sources of bibliographic data as in Figure 4.

Sr/Y crustal source at 5-10 kbar, fractionation of Sr-rich and Y-poor amphibole (± apatite) at shallow depths, or fractionation of garnet and Mg-rich amphibole at high pressure.

In the genesis of Tafresh adakites, garnet and amphibole seem to have both played some role. As for the first, the crucial observation is the depletion in HREE with respect to both LREE and MREE, given the well known preferential partitioning of HREE within garnet lattice (i.e., $^{garnet/melt}D_{HREE}$ >60; e.g., Taylor et al., 2015). On the other hand, the depletion of MREE, which are preferentially partitioned in amphibole (see previous section), with respect to LREE, is the best evidence for the latter. Although the common presence of amphibole in the intermediate Tafresh rocks renders fractionation of this phase a likely process, no evidence has ever been reported for garnet fractionation. This suggests that Tafresh adakites originated from the melting of a mafic source rock with residual garnet and amphibole, possibly represented by the metamorphosed subducted slab or by the lower continental crust. Since there is no geochemical parameter that could help to unequivocally assess which of the above two sources could be the most likely, some clues in this sense could be tentatively retrieved by taking into account the overall geodynamic setting in which Tafresh rocks have been emplaced. This is discussed more in detail in the following section.

Geodynamic implications

The investigated rocks from the Tafresh area display a large variety of petrographic and geochemical features attesting for numerous magmatic processes, including genesis and differentiation of "normal" subduction-related subalkaline series (from a variably metasomatized peridotite mantle source), genesis of subordinate magmas with adakitic signature and of crustal anatectic strongly evolved magmas. Such large variability is common in post-collisional geodynamic settings (e.g., Prelević and Seghedi, 2013; Couzinié et al., 2016; Fedele et al., 2016), which is thus the most likely scenario for the emplacement of the studied rocks. This is also in line with geochronological data for the onset of continent collision in NW/central UDMA around 22-16 Ma, although the range of ages obtained for the rocks from the Tafresh area (~57-15 Ma) suggests that magmatism developed also during pre-collisional stages. Within this framework, of particularly interest is the occurrence of rocks with adakitic signature throughout the UDMA. The genesis of such magmas is classically retained to mark the final stages of the subduction process or even the stages immediately following the onset of continental collision, being thus ascribed to melting of the subducted oceanic lithosphere during a post-collisional phase (adakites from Tabriz, Marand and Jolfa, NW UDMA, Isfahan, central UDMA, Dehaj, SE UDMA; Jahangiri, 2007; Khodami et al., 2009; Shaker Ardakani, 2016), a slab break-off (Anar, central/SW UDMA; Omrani et al., 2008) or a slab roll-back event (Tafresh and Nain, central/NW UDMA; Ghorbani and Bezenjani, 2011; Yeganehfar et al., 2013; Ghorbani et al., 2014). A few reports of rocks with adakitic signatures related to deep-level fractionation have been also documented for NW (Sanandaj, Upper Miocene; Azizi et al., 2014), central (Yazd Province, Pliocene-Quaternary; Sherafat et al., 2012) and SE UDMA (Kerman, Middle Miocene; Alirezaei et al., 2017).

More recently, Pang et al. (2016) questioned the slab melting models, proposing that Pleistocene Anar adakites are the product of the melting of lower crustal cumulates (metamorphosed to eclogite-facies rocks). These mafic lithologies were possibly induced to partially melt by the thermal perturbations associated with the post-collisional magmatism of Iran. The increase of the geothermal gradient was ascribed either to asthenospheric upwelling associated to the formation of a slab window or to lithospheric thickening during collision. Such alternative model, which was also proposed by Torkian et al. (2018) and by Kheirkhah (2020) for the genesis of the Miocene adakites from NW UDMA (Sheyda volcano) and of the adakites from Dehaj (SE UDMA), respectively, seems consistent with the collisional setting in which the studied Tafresh adakites were likely emplaced.

Nevertheless, since post-Eocene igneous rocks from the Tafresh area have been emplaced during a time lapse from pre- to post-collisional stages, the slab break-off and slab roll-back hypotheses could not be definitively rejected. This is even more evident in the light of the very recent recognition of pre-collisional (Paleocene, ~58-56 Ma) granitoids with adakitic signature in NW UDMA (Saqqez-Takab), which Azizi et al. (2019) ascribed to the partial melting of lower crustal rocks due to the asthenospheric upwelling related with slab roll-back (or even to deep-level amphibole fractionation of "normal" calcalkaline magmas). In the light of the previously recalled progressive inception of the continental collision moving from NW to SE, it could be also reasonable to hypothesize that more than just a single kind of process could have been active to produce the UDMA adakites. Further studies on these rocks are thus needed, including detailed petrochemical characterization and accurate absolute age data.

CONCLUSIONS

Igneous rocks from the Tafresh area of the UDMA testify for widespread Cenozoic magmatism resulting in a large spectrum of rock types, variably affected by secondary processes. Most of the investigated igneous products, ranging in composition from weakly evolved to evolved lithotypes (with intermediate andesitic rock types being the most common) likely belong to a calcalkaline suite with orogenic affinity.

Primitive magmas (not represented in the geological record) likely originated from a peridotite mantle source, previously metasomatized by addition of subduction-related fluids (as indicated by the typical LILE-enriched and HFSE-depleted geochemical signature), which melted in the spinel stability field. Differentiation processes were mainly driven by fractional crystallization of 1) ferromagnesian minerals (mostly clinopyroxene and olivine) and plagioclase, 2) plagioclase and amphibole, and finally 3) plagioclase and alkali feldspars, in good accordance with both petrographic and whole-rock geochemical evidence.

Additional rock types include rarer evolved rocks with adakitic geochemical fingerprint (Sr-enriched and Y- and HREE-depleted) and leucocratic peraluminous strongly evolved rocks. The first are ascribed to melting of a meta-mafic source rock (either the subducting oceanic slab or the lower continental crust) leaving a garnet and amphibole-bearing residue, while the second are likely the product of the anatexis of a mixed meta-sedimentary (i.e., including both pelitic and greywacke lithologies) crustal source.

The association of such a large variety of magma types in a relatively narrow area is consistent with a post-collisional geodynamic setting, although additional more detailed petrological investigations are still considered necessary in order to unequivocally elucidate the complex geodynamic scenario of the investigated area.

ACKNOWLEDGEMENTS

This research is part of the PhD project of the first author. ML thanks Ateneo La Sapienza for research funds (2016, 2017, 2018). ML and SA acknowledge PRIN 2018 funds. The official revision of Ahmad Rabiee and the comments from the editor Silvio Mollo were greatly appreciated.

REFERENCES

Agard P., Omrani J., Jolivet L., Mouthereau F., 2005. Convergence history across Zagros (Iran): constraints from collisional and earlier deformation. International Journal of Earth Science 94, 401-419.

Agard P., Omrani J., Jolivet L., Whitechurch H., Vrielynck B., Spakman W., Monié P., Meyer B., Wortel R., 2011. Zagros orogeny: a subduction-dominated process. Geological Magazine 148, 692-725.

Ahmadzadeh G., Jahangiri A., Lentz D., Mojtahedi M., 2010. Petrogenesis of Plio-Quaternary post-collisional ultrapotassic volcanism in NW of Marand, NW Iran. Journal of Asian Earth Science 39, 37-50.

Alirezaei A., Arvin M., Dargahi S., 2017. Adakite-like signature of porphyry granitoid stocks in the Meiduk and Parkam porphyry copper deposits, NE of Shahr-e-Babak, Kerman, Iran: constrains on geochemistry. Ore Geology Reviews 88, 370-83.

Allen M.B., Kheirkhah M., Neill I., Emami M.H., Mcleod C.L., 2013. Generation of arc and within-plate chemical signatures in collision zone magmatism: Quaternary lavas from Kurdistan Province, Iran. Journal of Petrology 54, 887-911.

Arvin M., Pan Y., Dargahi S., Malekizadeh A., Babaei A., 2007. Petrochemistry of the Siah-Kuh granitoid stock southwest of Kerman, Iran: Implications for initiation of Neotethys

subduction, Journal of Asian Earth Science 30, 474-489.

Asiabanha A. and Foden J., 2012. Post-collisional transition from an extensional volcano-sedimentary basin to a continental arc in the Alborz Ranges, N-Iran. Lithos 148, 98-111.

Azizi H., Asahara Y., Tsuboi M., Takemura K., Razyani S., 2014. The role of heterogenetic mantle in the genesis of adakites northeast of Sanandaj, northwestern Iran. Chemie der Erde 74, 87-97.

Azizi H., Stern R.J., Topuz G., Asahara Y., Shafaii Moghadam H., 2019. Late Paleocene adakitic granitoid from NW Iran and comparison with adakites in the NE Turkey: adakitic melt generation in normal continental crust. Lithos 346-347, 105151.

Azizi H., Tanaka T., Asahara Y., Chung S.-L., Zarrinkoub M.H., 2011. Discrimination of the age and tectonic setting for magmatic rocks along the Zagros thrust zone, northwest Iran, using the zircon U-Pb age and Sr-Nd isotopes. Journal of Geodynamics 52, 304-320.1

Bagheri S. and Stampfli G.M., 2008. The Anarak, Jandaq and Posht-e-Badam metamorphic complexes in central Iran: new geological data, relationships and tectonic implications. Tectonophysics 451, 123-155.

Bellver-Baca M.T., Chiaradia M., Beate B., Beguelin P., Deriaz B., Mendez-Chazarra N., Villagómez D., 2020. Geochemical evolution of the Quaternary Chachimbiro Volcanic Complex (frontal volcanic arc of Ecuador). Lithos 356-357, 105237.

Berberian F. and Berberian M., 1981. Tectono-plutonic episodes in Iran. In: Gupta H.K., Delany F.M. (Eds.), Zagros, Hindu Kush, Himalaya: Geodynamic Evolution volume 3. American Geophysical Union, Washington D.C., pp. 5-32.

Berberian M. and King G.C.P., 1981. Towards a paleogeography and tectonic evolution of Iran. Canadian Journal of Earth Science 18, 210-265.

Boccaletti M., Innocenti F., Manetti P., Mazzuoli R., Motamed A., Pasquare G., Radicati di Brozolo F., Sobhani E.A., 1977. Neogene and quaternary volcanism of the Bijar Area (Western Iran). Bulletin of Volcanology 40, 121-132.

Breitfeld H.T., Macpherson C., Hall R., Thirlwall M., Ottley C.J., Hennig-Breitfeld J., 2019. Adakites without a slab: remelting of hydrous basalt in the crust and shallow mantle of Borneo to produce the Miocene Sintang Suite and Bau Suite magmatism of West Sarawak. Lithos 344-345, 100-121.

Burg J.-P., 2018. Geology of the onshore Makran accretionary wedge: synthesis and tectonic interpretation. Earth-Science Reviews 185, 1210-1231.

Carminati E., Lustrino M., Doglioni C., 2012. Geodynamic evolution of the central and western Mediterranean: Tectonics vs igneous petrology constraints. Tectonophysics 579, 173-192.

Castillo P.R., 2012. Adakite petrogenesis. Lithos 134-135, 304-316.

Chappell B.W., 1999. Aluminium saturation in I- and S-type granites and the characterization of fractionated haplogranites. Lithos 46, 535-551.

Chappell B.W., Bryant C.J., Wyborn D., 2012. Peraluminous I-type granites. Lithos 153, 142-153.

Chappell B.W. and White J.R., 2001. Two contrasting granite types: 25 years later. Australian Journal of Earth Sciences 48, 489-499.

Chiu H.-Y., Chung S.-L., Zarrinkoub M.H., Mohammadi S.S., Khatib M.M., Iizuka Y., 2013, Zircon U-Pb age constraints from Iran on the magmatic evolution related to Neotethyan subduction and Zagros orogeny: Lithos 162-163, 70-87.

Chung S.-L., Liu D., Ji J., Chu M.-F., Lee H.-Y., Wen D.-J., Lo C.-H., Lee T.-Y., Qian Q., Zhang Q., 2003. 2003. Adakites from continental collision zones: Melting of thickened lower crust beneath southern Tibet. Geology 31, 1021-1024.

Clemens J.D. and Stevens G., 2012. What controls chemical variation in granitic magmas? Lithos 134-135, 317-329.

Clemens J.D., Stevens G., Farina F., 2011. The enigmatic source of I-type granites: the peritectic connection. Lithos 126, 174-181.

Couzinié S., Laurent O., Moyen J.-F., Zeh A., Bouilhol P., Villaros A., 2016. Post-collisional magmatism: crustal growth not identified by zircon Hf-O isotopes. Earth and Planetary Science Letters 456, 182-195.

Davidson J., Hassanzadeh J., Berzins R., Stockli D.F., Bashukooh B., Turrin B., Pandamouz A., 2004. The geology of Damavand volcano, Alborz Mountains, northern Iran. Geological Society of America Bulletin 116, 16-29.

Deevsalar R., Shinjo R., Ghaderi M., Murata M., Hoskin P.W.O., Oshiro S., Neill I., 2017. Mesozoic-Cenozoic mafic magmatism in Sanandaj-Sirjan Zone, Zagros Orogen (Western Iran): geochemical and isotopic inferences from Middle Jurassic and Late Eocene gabbros. Lithos 284-285, 588-607.

Defant M.J. and Drummond M.S., 1990. Derivation of some modern arc magmas by melting of young subducted lithosphere. Nature 347, 662-665.

Di Giuseppe P., Agostini S., Lustrino M., Karaoğlu O., Savaşçin M.Y., Manetti P., Ersoy Y., 2017. Transition from compression to strike-slip tectonics revealed by Miocene-Pleistocene volcanism west of the Karliova Triple Junction (East Anatolia). Journal of Petrology 58, 2055-2087.

Drummond M.S. and Defant M.J., 1990. A model for trondhjemite-tonalite-dacite genesis and crustal growth via slab melting: Archaean to modern comparisons. Journal of Geophysical Research 95, 21503-21521.

Faccenna C., Becker T.W., Auer L., Billi A., Boschi L., Brun J.P., Capitanio F.A., Funiciello F., Horvath F., Jolivet L., 2014. Mantle dynamics in the Mediterranean. Reviews of Geophysics 52, 283-332.

Fazlnia A., 2019. Origin and magmatic evolution of the Quaternary syn-collision alkali basalts and related rocks from Salmas, northwestern Iran. Lithos 344-345, 297-310.

Fedele L., Seghedi I., Chung S.-L., Laiena F., Lin T.-H., Morra

V., Lustrino M., 2016. Post-collisional magmatism in the Late Miocene Rodna-Bârgău district (East Carpathians, Romania): Geochemical constraints and petrogenetic models. Lithos 266-267, 367-382.

Ghorbani M.R. and Bezenjani R.N., 2011. Slab partial melts from the metasomatizing agent to adakite, Tafresh Eocene volcanic rocks, Iran. Island Arc 20, 188-202.

Ghorbani M.R., Graham I.T., Ghaderi M., 2014. Oligocene-Miocene godynamic evolution of the central part of the Urumieh-Dokhtar Arc of Iran. International Geology Review 56, 1039-1050.

Hajian J., 1970. Geological Map of the Farmahin. Geological Survey of Iran, Scale 1:100,000.

Hajian J., 1977. Geological Map of the Tafresh Area: Tehran. Geological Survey of Iran, Scale 1:100,000.Hajian J., 2001. Geology of Tafresh: Tehran. Geological and Mineralogical Exploration Survey of Iran, report 82.

Hassanzadeh J., Stockli D.F., Horton B.K., Axen G.J., Stockli L.D., Grove M., Schmitt A.K., Walker J.D., 2008. U-Pb zircon geochronology of late Neoproterozoic-Early Cambrian granitoids in Iran: Implications for paleogeography, magmatism, and exhumation history of Iranian basement. Tectonophysics 451, 71-96.

Hassanzadeh J. and Wernicke B.P., 2016. The Neotethyan Sanandaj-Sirjan zone of Iran as an archetype for passive margin-arc transitions. Tectonics 35, 586-621.

Hastie A.R., Kerr A.C., Pearce J.A., Mitchell S.F., 2007. Classification of altered volcanic island arc rocks using immobile trace elements: development of theTh-Co discrimination diagram. Journal of Petrology 48, 2341-2357.

Honarmand M., Omran N.R., Neubauer F., Emami M.H., Nabatian G., Liu X., Dong Y., von Quadt A., Chen B., 2014. Laser-ICP-MS U-Pb zircon ages and geochemical and Sr-Nd-Pb isotopic compositions of the Niyasar plutonic complex, Iran: constraints on petrogenesis and tectonic evolution. International Geology Review 56, 104-132.

Horton B.K., Hassanzadeh J., Stockli D.F., Axen G.J., Gillis R.J., Guest B., Amini A.H., Fakhari M., Zamanzadeh S.M., Grove M., 2008. Detrital zircon provenance of Neoproterozoic to Cenozoic deposits in Iran: implications for chronostratigraphy and collisional tectonics. Tectonophysics 451, 97-122.

Jagoutz O. and Klein B., 2018. On the importance of crystallization-differentiation for the generation of SiO_2-rich melts and the compositional build-up of arc (and continental) crust. American Journal of Science 318, 29-63.

Jahangiri A., 2007. Post-collisional Miocene adakitic volcanism in NW Iran: Geochemical and geodynamic implications. Journal of Asian Earth Science 30, 433-447.

Kamei A., Miyake Y., Owada M., Kimura J., 2009. A pseudo adakite derived from partial melting of tonalitic to granodioritic crust, Kyushu, southwest Japan arc. Lithos 112, 615-625.

Karaoğlu O., Gulmez F., Goçmengil G., Lustrino M., Di Giuseppe P., Manetti P., Savasçin M.Y., Agostini S., 2020. Petrological evolution of Karliova-Varto volcanism (Eastern Turkey): magma genesis in a transtensional triple-junction tectonic setting. Lithos, 364-365, 105524.

Karasözen E., Nissen E., Bergman E.A., Ghods A., 2019. Seismotectonics of the Zagros (Iran) from orogen-wide, calibrated earthquake relocations. Journal of Geophysical Research: Solid Earth 124, 9109-9129.

Khademi F., Asiabanha A., Foden J., Davoodi Z., 2019. Extensional magmatism in a continental collision zone, Tafresh area, western central Iran: structural, geochemical and mineralogical considerations. Periodico di Mineralogia 88, 1-18.

Kheirkhah M., Allen M.B., Emami M., 2009. Quaternary syn-collision magmatism from the Iran/Turkey borderlands. Journal of Volcanology and Geothermal Research 182, 1-12.

Kheirkhah M., Neill I., Allen M.B., Ajdari K., 2013. Small-volume melts of lithospheric mantle during continental collision: late Cenozoic lavas of Mahabad, NW Iran. Journal of Asian Earth Science 74, 37-49.

Kheirkhah M., Neill I., Allen M.B., Emami, M.H., Shahraki Ghadimi A., 2020. Distinct sources for high-K and adakitic magmatism in SE Iran. Journal of Asian Earth Science, 196, 104355.

Khodami M., Noghreyan M., Davoudian A.R., 2009. Pliocene-Quaternary adakite volcanism in the Isfahan area, Central Iranian magmatic belt. Neues Jahrbuch für Mineralogie Abhandlungen 186, 235-248.

King A.J., Phillips K.J.H., Vita-Finzi C., Russell S.S., 2020. Terrestrial modification of the Ivuna meteorite and a reassessment of the chemical composition of the CI type specimen. Geochimica et Cosmochim. Acta 268, 73-89.

Koshnaw R.I., Stockli D.F., Schlunegger F., 2018. Timing of the Arabia-Eurasia continental collision - evidence from detrital zircon U-Pb geochronology of the Red Bed Series strata of the northwest Zagros hinterland, Kurdistan region of Iraq. Geology 47, 47-50.

Le Maitre R.W. (Ed.), 2002. Igneous Rocks: A Classification and Glossary of Terms. Recommendations of the International Union of Geological Sciences Subcommission on the Systematics of Igneous Rocks. Cambridge University Press, Cambridge, UK, pp. 256.

Liu J., Xie C., Li C., Fan J., Wang M., Wang W., Yu Y., Dong Y., Hao Y., 2019. Origins and tectonic implications of Late Cretaceous adakite and primitive high-Mg andesite in the Songdo area, southern Lhasa subterrane, Tibet. Gondwana Research 76, 185-203.

Lustrino M., Keskin M., Mattioli M., Lebedev V.A., Chugaev A., Sharkov E., Kavak O., 2010. Early activity of the largest Cenozoic shield volcano in the circum-Mediterranean area: Mt. Karacadağ, SE Turkey. European Journal of Mineralogy 22, 343-362.

Lustrino M., Fedele L., Agostini S., Prelević D., Salari G., 2019.

Leucitites within and around the Mediterranean area. Lithos 324-325, 216-233.

Lyubetskaya T. and Korenaga J., 2007. Chemical composition of Earth's primitive mantle and its variance: 1. Methods and results. Journal of Geophysical Research 112, B03211. doi: 10.1029/2005JB004223.

Ma Q., Zheng J., Griffin W.L., Zhang M., Tang H., Su Y., Ping X., 2012. Triassic "adakitic" rocks in an extensional setting (North China): Melts from the cratonic lower crust. Lithos 149, 159-173.

Maanijou M., Aliani F., Miri M., Lentz D.R., 2013. Geochemistry and petrology of igneous assemblage in the south of Qorveh area, west Iran. Chemie der Erde 73, 181-196.

Macpherson C.G., Dreher S.T., Thirlwall M.F., 2006. Adakites without slab melting: High pressure differentiation of island arc magma, Mindanao, the Philippines. Earth and Planetary Science Letters 243, 581-593.

Mahmoudi S., Corfu F., Masoudi F., Mehrabi B., Mohajjel M., 2011. U-Pb dating and emplacement history of granitoid plutons in the northern Sanandaj-Sirjan Zone, Iran. Journal of Asian Earth Science 41, 238-249.

Martin H., Smithies R.H., Rapp R., Moyen J.-F., Champion D., 2005. An overview of adakite, tonalite-trondhjemite-granodiorite (TTG), and sanukitoid: relationships and some implications for crustal evolution. Lithos 79, 1-24.

Masson F.D.R., Anvari M., Djamour Y., Walpersdorf A., Tavakoli F., Daignières M., Nankali H., Van Gorp S.B., 2007. Large-scale velocity field and strain tensor in Iran inferred from GPS measurements: new insight for the present-day deformation pattern within NE Iran. Geophysical Journal International 170, 436-40.

Mazhari S.A., Bea F., Amini S., Ghalamghash J., Molina J.F., Montero P., Scarrow J.H., Williams I.S., 2009. The Eocene bimodal Piranshahr massif of the Sanandaj-Sirjan Zone, NW Iran: a marker of the end of the collision in the Zagros orogen. Journal of the Geological Society, London 166, 53-69.

McQuarrie N. and van Hinsbergen D.J., 2013. Retrodeforming the Arabia-Eurasia collision zone: age of collision versus magnitude of continental subduction. Geology 41, 315-318.

Melekhova E., Blundy J., Robertson R., Humphreys M.C.S., 2015. Experimental evidence for polybaric differentiation of primitive arc basalt beneath St. Vincent, Lesser Antilles. Journal of Petrology 56, 161-192.

Molinaro M., Leturmy P., Guezou J.C., Frizon de Lamotte D., Eshraghi S.A., 2005. The structure and kinematics of the southeastern Zagros fold–thrust belt, Iran: from thin-skinned to thick-skinned tectonics. Tectonics 24. doi: 10.1029/2004TC001633.

Mouthereau F., Lacombe O., Meyer B., 2006. The Zagros folded belt (Fars, Iran): constraints from topography and critical wedge modelling. Geophysical Journal International 165, 336-356.

Mouthereau F., Lacombe O., Vergés J., 2012. Building the Zagros collisional orogen: Timing, strain distribution and the dynamics of Arabia/Eurasia plate convergence. Tectonophysics 532-535, 27-60.

Moyen J.-F., 2009. High Sr/Y and La/Yb ratios: the meaning of the "adakitic signature". Lithos 112, 556-574.

Nandedkar R.H., Hürlimann N., Ulmer P., Müntener O., 2016. Amphibole-melt trace element partitioning of fractionating calcalkaline magmas in the lower crust: an experimental study. Contributions to Mineralogy and Petrology 171, 71. doi: 10.1007/s00410-016-1278-0.

Neill I., Meliksetian K., Allen M.B., Navasardyan G., Kuiper K., 2015. Petrogenesis of mafic collision zone magmatism: the Armenian sector of the Turkish-Iranian Plateau. Chemical Geology 403, 24-41.

Omrani J., Agard P., Whitechurch H., Benoit M., Prouteau G., Jolivet L., 2008. Arc-magmatism and subduction history beneath the Zagros Mountains, Iran: a new report of adakites and geodynamic consequences. Lithos 106, 380-398.

Palin R.M., White R.W., Green E.C.R., 2016. Partial melting of metabasic rocks and the generation of tonalitic-trondhjemitic-granodioritic (TTG) crust in the Archaean: Constraints from phase equilibrium modelling. Precambrian Research 287, 73-90.

Pang K.-N., Chung S.-L., Zarrinkoub M.H., Khatib M.M., Mohammadi S.S., Chiu H.-Y., Chu C.-H., Lee H.-Y., Lo C.-H., 2013. Eocene-Oligocene post-collisional magmatism in the Lut-Sistan region, eastern Iran: magma genesis and tectonic implications. Lithos 180-181, 234-251.

Pang K.-N., Chung S.-L., Zarrinkoub M.H., Li X.-H., Lee H.-Y., Lin T.-H., Chiu H.-Y., 2016. New age and geochemical constraints on the origin of Quaternary adakite-like lavas in the Arabia-Eurasia collision zone. Lithos 264, 348-359.

Pearce J.A., Bender J.F., Delong S.E., Kidd W.S.F., Low P.J., Guner Y., Sargolu F., Yilmaz Y., Moorbath S., Mitchell J.G., 1990. Genesis of collision volcanism in eastern Anatolia, Turkey. Journal of Volcanology and Geothermal Research 44, 189-229.

Pichavant M., Martel C., Bourdier J.-L., Scaillet B., 2002. Physical conditions, structure and dynamics of a zoned magma chamber: Mount Pelée (Martinique, Lesser Antilles Arc). Journal of Geophysical Research 107, B5, 2093.doi: 10.1029/2001JB000315.

Plank T., 2014. The chemical composition of subducting sediments. In: Holland H.D., Turekian K.K. (Eds.), Treatise on Geochemistry, second edition. Volume 4: The Crust. Elsevier, Oxford, pp. 607-629.

Prelević D. and Seghedi I., 2013. Magmatic response to the post-accretionary orogenesis within Alpine-Himalayan belt - preface. Lithos 180-181, 1-4.

Prowatke S. and Klemme S., 2006a. Trace element partitioning between apatite and silicate melts. Geochimica and Cosmochimica Acta 70, 4513-4527.

Prowatke S. and Klemme S., 2006b. Rare Earth element

partitioning between titanite and silicate melts: Henry's Law revisited. Geochimica et Cosmochimica Acta 70, 4997-5012.

Rabiee A., Rossetti F., Asahara Y., Azizi H., Lucci F., Lustrino M., Noazem R., 2020. Long-lived, Eocene-Miocene stationary magmatism in NW Iran along a transform plate boundary. Gondwana Research 85, 237-262.

Raeisi D., Mirnejad H., Sheibi M., 2019. Emplacement mechanism of the Tafresh granitoids, central part of the Urumieh-Dokhtar Magmatic Arc, Iran: evidence from magnetic fabrics. Geological Magazine 156, 1510-1526.

Ribeiro J.M., Maury R.C., Grégoire M., 2016. Are adakites slab melts or high-pressure fractionated mantle melts? Journal of Petrology 57, 839-862.

Richards J. and Kerrich R., 2007. Special paper: Adakite-like rocks: their diverse origins and questionable role in metallogenesis. Economic Geology 102, 537-576.

Riou R., Dupuy C., Dostal J., 1981. Geochemistry of coexisting alkaline and calc-alkaline volcanic rocks from northern Azerbaijan (N.W. Iran). Journal of Volcanological and Geothermal Research 11, 253-275.

Rodríguez C., Sellés D., Dungan M., Langmuir C., Leeman W., 2007. Adakitic dacites formed by intracrustal crystal fractionation of water-rich parent magmas at Nevado de Longav Volcano (36.28°S; Andean Southern Volcanic Zone, Central Chile). Journal of Petrology 11, 2033-2061.

Rudnick R.L. and Gao S., 2014. Composition of the continental crust. In: Holland H.D., Turekian K.K. (Eds.), Treatise on Geochemistry, second edition. Volume 4: The Crust. Elsevier, Oxford, pp. 1-51.

Sengör A.M.C., Altiner D., Cin A., Ustaömer T., Hsü K.J., 1988. Origin and assembly of the Tethysides orogenic collage at the expense of Gondwana Land. In: Audley-Charles M.G., Hallam A. (Eds.), Gondwana and Tethys. Geological Society London Special Publications 37, 119-181.

Shahbazi H., Siebel W., Pourmoafee M., Ghorbani M., Sepahi A.A., Shang C.K., Abedini M.V., 2010. Geochemistry and U-Pb zircon geochronology of the Alvand plutonic complex in Sanandaj-Sirjan Zone (Iran): new evidence for Jurassic magmatism. Journal of Asian Earth Science 39, 668-683.

Shaker Ardakani A., 2016. Post-collisional Plio-Pleistocene Anar-Dehaj adakitic subvolcanic domes in the central volcanic belt of Iran: geochemical characteristics and tectonic implications. Periodico di Mineralogia 85, 185-200.

Sherafat S., Yavuz F., Noorbehesht I., Yıldırım D.K., 2012. Mineral chemistry of Plio-Quaternary subvolcanic rocks, southwest Yazd Province, Iran. Int Geol Rev 54, 1497-1531.

Stampfli G.M., Hochard C., Vérard C., Wilhem C., vonRaumer J., 2013. The formation of Pangea. Tectonophysics 593, 1-19.

Sylvester P.J., 1998. Strongly peraluminous granites. Lithos 45, 29-44.

Taylor R.J.M., Harley S.L., Hinton R.W., Elphick S., Clark C., Kelly N.M., 2015. Experimental determination of REE partition coefficients between zircon, garnet and melt: a key to understanding high-T crustal processes. Journal of Metamorphic Geology 33, 231-248.

Torkian A., Furman T., Salehi N., Veloski K., 2018. Petrogenesis of adakites from the Sheyda volcano, NW Iran. Journal of African Earth Science 150, 194-204.

Van Hinsbergen D.J.J., Lippert P.C., Li S., Huang W., Advokaat E.L., Spakman W., 2019. Reconstructing Greater India: paleogeographic, kinematic, and geodynamic perspectives. Tectonophysics 760, 69-94.

Van Hinsbergen D.J.J., Torsvik T.H., Schmid S.M., Matenco L.C., Maffione M., Vissers R.L.M., Gurer D., Spakman W., 2020. Orogenic architecture of the Mediterranean region and kinematic reconstructions of its tectonic evolution since the Triassic. Gondwana Research 81, 79-229.

Verdel C., Wernicke B.P., Hassanzadeh J., Guest B., 2011. A Paleogene extensional arc flare-up in Iran. Tectonics 30, TC3008. doi: 10.1029/2010TC002809.

Walker R.T., Gans P., Allen M.B., Jackson J., Khatib M., Marsh N., Zarrinkoub M., 2009. Late Cenozoic volcanism and rates of active faulting in eastern Iran. Geophysical Journal International 177, 783-805.

Wilmsen M., Fürsich F.T., Seyed-Emami K., Majidifard M.R., Taheri J., 2009. The Cimmerian Orogeny in northern Iran: Tectonostratigraphic evidence from the foreland. Terra Nova 21, 211-218.

Winchester J.A. and Floyd P.A., 1977. Geochemical discrimination of different magma series and their differentiation products using immobile elements. Chemical Geology 20, 325-343.

Wang Q., Xu J.-F., Jian P., Bao Z.-W., Zhao Z.-H., Li C.-F., Xiong X.-L., Ma J.-L., 2006. Petrogenesis of adakitic porphyries in an extensional tectonic setting, Dexing, South China: implications for the genesis of porphyry copper mineralization. Journal of Petrology 47, 119-144.Zheng Y.-F., 2019. Subduction zone geochemistry. Geoscience Frontiers 10, 1223-1254.

Yeganehfar H., Ghorbani M.R., Shinjo R., Ghaderi M., 2013. Magmatic and geodynamic evolution of Urumieh-Dokhtar basic volcanism, Central Iran: major, trace element, isotopic, and geochronologic implications. International Geology Review 55, 767-786.